FLSEVIER

Contents lists available at SciVerse ScienceDirect

Journal of Non-Newtonian Fluid Mechanics

journal homepage: http://www.elsevier.com/locate/jnnfm



Shear-induced particle migration: Predictions from experimental evaluation of the particle stress tensor



T. Dbouk ^a, E. Lemaire ^b, L. Lobry ^b, F. Moukalled ^{c,*}

- ^a MINES ParisTech, Centre de Mise en Forme des matériaux (CEMEF), 1 Rue Claude Daunesse, 06904 Sophia Antipolis Cedex, France
- ^b Laboratoire de Physique de la Matière Condensée, LPMC, UMR 7336, Parc Valrose, 06108 Nice Cedex 2, France
- ^c American University of Beirut (AUB), Department of Mechanical Engineering, P.O. Box 11-0236, Riad El-Solh, Beirut 1107 2020, Lebanon

ARTICLE INFO

Article history: Received 11 December 2012 Received in revised form 4 March 2013 Accepted 6 March 2013 Available online 16 May 2013

Keywords: Monodispersed flow Particle migration Suspension balance model Finite volume method OpenFOAM®

ABSTRACT

This paper addresses the modeling of the phenomenon of particle migration in the flow of monodispersed non-colloidal suspensions at neglected inertia using the Suspension Balance Model (SBM). The SBM describes the migration flux of particles as the divergence of the particle stress tensor. It is selected in this work because of its parameters that can be measured experimentally and its capability to quantify well the shear-induced migration phenomenon. A recent experiment [10,11] reported measurements of the different parameters in the SBM, which are used in this work to study their effects on the prediction of the particle migration phenomenon. For that purpose, a two-dimensional solver capable of solving the set of conservation equations of the SBM using the finite volume method is developed within the "OpenFOAM®" CFD toolbox [34]. The code is validated by simulating the suspension flows in a channel of rectangular cross-section, and in a wide gap Couette cell. Solutions are generated using the newly measured SBM parameters, and results are compared to similar ones obtained using the old SBM parameters. It is found that the new measured parameters have no significant influence on prediction of particle migration as compared to those proposed in the literature. Finally, the SBM is extended to general two-dimensional flows through a frame-invariant formulation that takes into account the local kinematics of the suspension including buoyancy effects. The frame-invariant model is applied to the resuspension and mixing of a monodispersed suspension in a horizontal Couette cell. The predicted results are found to be in good agreement with experimental measurements.

© 2013 Elsevier B.V. All rights reserved.

1. Introduction

The flow of non-Brownian suspensions has captured a lot of attention over the past few decades as reflected by the numerous studies on the subject conducted since the 1970s. These suspensions are used in our daily life in many products like paints, cosmetics, and detergents. They are also observed in a variety of natural phenomena like mud, fuel, and rivers. This work is concerned with the numerical modeling of monodispersed non-colloidal suspensions made of hard spheres immersed in a Newtonian liquid at neglected inertia ($Re \ll 1$).

Abbreviations: SBM, Suspension Balance Model; NMR, Nuclear Magnetic Resonance; PIV, Particle Image Velocimetry; LDV, Laser Doppler Velocimetry; SIDM, Shear Induced Diffusion Model; FVM, Finite Volume Method; SD, Stokesian Dynamics.

E-mail addresses: talib.dbouk@mines-paristech.fr (T. Dbouk), elisabeth.lemair-e@unice.fr (E. Lemaire), laurent.lobry@unice.fr (L. Lobry), memouk@aub.edu.lb (F. Moukalled).

The task of modeling concentrated suspensions is a hard one complicated by the multi-body interactions that have to be taken into account in order to represent well the observed shear-induced migration phenomenon. This migration behavior can be seen in the form of inhomogeneous distribution of particles whenever a homogeneous suspension is sheared. Therefore understanding the inhomogeneity of particles distribution in such flows is essential and crucial for understanding and accurately predicting various industrial processes.

Many experimental studies have been performed to characterize the shear-induced particle migration and to identify the mechanisms responsible for it. Measurements taken in different geometrical configurations (Concentric Couette Cell, cone-plate, two parallel-disks, channels, etc.) [17,7,36,23,25] demonstrate that the particles generally migrate from high shear-rate zones to low shear-rate ones. For example in the Couette cell geometry, measurements of the particle concentrations obtained using different techniques (e.g. the Nuclear Magnetic Resonance NMR, Particle Image Velocimetry PIV, and Laser Doppler Velocimetry LDV) indicate the presence of radial migration from zones of high shear rate near

^{*} Corresponding author. Tel.: +961 3831432.

ı	particle radius	\mathbf{U}^p	mean velocity vector of the particle phase
le	Reynold's number	E	strain rate tensor
	volume fraction of particles	$oldsymbol{\Sigma}$	suspension stress tensor
b	bulk volume fraction of particles	$\boldsymbol{\Sigma}^f$	fluid stress tensor
m	maximum packing volume fraction	$\mathbf{\Sigma}^p$	oriented particle stress tensor
	shear rate	$\mathbf{\Sigma}^{p}$	general particle stress tensor
I_1	first normal stress difference	\mathbf{F}^H	hydrodynamic force
I_2	second normal stress difference	П	particle pressure
l	suspension dynamic viscosity	Q	diagonal tensor of the suspension balance model
	suspension kinematic viscosity	v_{stokes}	Stokes settling velocity
s	normalized suspension viscosity	g	gravitational acceleration vector
0	suspending liquid viscosity	P_f	fluid pressure
V	normal stress viscosity	p	total pressure
p	shear viscosity of the particle phase	n	density number of particles
e_p	particles Reynold's number	$f(\phi)$	sedimentation Hindrance function
e	Pelclet's number	α	fitting parameter in $f(\phi)$
T	thermal energy	λ_2	parameter of the SBM
)	suspension density	λ_3	parameter of the SBM
$_0, ho_f$	fluid density	K_N	parameter of the SBM
р	particle density	t	time
	migration flux	Cr	Courant number

the inner rotating cylinder toward regions of low shear rate near the outer stationary cylinder.

Two approaches have been followed in developing models for predicting particle migration in sheared suspensions, which are denoted in the literature by the "shear induced diffusion model" (SIDM) and the "Suspension Balance Model" (SBM). In the phenomenological SIDM [20,21,36] migration is predicted based on the net displacement of particles during collisions. This model, which proposes that this migration is the result of two fluxes induced by gradients of both collision rates and viscosity, is more phenomenological than quantitative as it introduces several diffusion coefficients that are not easy to obtain neither theoretically nor experimentally.

The SBM, adopted in this work, explains the particle migration following a path different than the one followed in SIDM and allows easier prediction of this phenomenon because most of its parameters can be measured experimentally. The SBM utilizes normal stresses in its formulation, a significant feature in a concentrated suspension subject to a shear flow that cannot be captured by SIDM. It was first proposed by Nott and Brady [32] and then used by Morris and Brady [30] in the presence of buoyancy forces, and later by Morris and Boulay [29], and was restricted to suspensions subjected to simple shear flows. Later Miller et al. [28] extended this Model to general two-dimensional flows taking into account the local kinematics of the suspension.

The physical concept in the SBM is that an inhomogeneous stress exists due to the particle phase inside the suspension during the flow. This stress forces the particles to migrate in order to balance that inhomogeneity. The SBM introduces a migration flux (\mathbf{j}) that is directly proportional to the divergence of the particle stress tensor $(\nabla \cdot \Sigma^p)$. This migration flux is due to variations in the concentration of particles (ϕ) in the suspension or shear rate gradients $(\dot{\gamma})$, which induce gradients in the particle stress. In other words, since $\Sigma^p = f(\phi, \dot{\gamma})$, if the concentration volume fraction is not uniform $(\phi \neq \text{constant})$ or if the shear rate is varying $(\dot{\gamma} \neq \text{constant})$ then a particle migration flux (\mathbf{j}) appears. The suspension stress (Σ) in the SBM is defined as the sum of both the particle stress Σ^p and the fluid stress $\Sigma^f(i.e.\Sigma = \Sigma^p + \Sigma^f)$.

The rheological measurements of the two "suspension normal stress differences" $N_1 = \Sigma_{11} - \Sigma_{22}$ and $N_2 = \Sigma_{22} - \Sigma_{33}$ and the "suspension viscosity" η_s , which are all material functions of the suspension, in addition to one normal component of the stress tensor (Σ_{11} , Σ_{22} , or Σ_{33}) allow the suspension stress tensor Σ to be completely evaluated. Knowing Σ , the fluid stress tensor Σ^f must be also measured to be able to determine the particle stress tensor Σ^p that is required in the SBM. Yet, reported experimental studies on N_1 and N_2 to calculate the suspension normal stress Σ and especially the Σ^p tensor are rare due to their simultaneous measuring complexity.

The work conducted by Gadala-Maria [16] showed that the difference of the normal stress differences $(N_1 - N_2)$ is proportional to the shear stress and that N_1 and N_2 are of the same order of magnitude. Zarraga et al. [48] determined both Normal stress differences N_1 and N_2 by exploiting the anti-Weissenberg effect and by measuring the total force exerted on a rotating cone or disk, on top of a stationary plane. Their measurements indicated that N_1 and N_2 are both negative and that $N_1 \sim \frac{N_2}{4}$. Later Singh and Nott [44] proposed a technique to measure both N_1 and N_2 by coupling data taken from two separate experiments. Results indicated that N_1 and N_2 are both negative, and that $N_1 \approx N_2$. Recently, Boyer et al. [3] using the anti-Weissenberg effect, reported on the variation of $(N_1 + 2N_2)$ as a function of ϕ . In addition, Couturier et al. [8] determined the second normal stress difference N_2 , by measuring the deformation of the free surface of a suspension flow in a narrow inclined channel. Both studies showed that N_1 is of the order of zero, and N_2 is negative.

All experimental studies dealing with the flow of monodispersed suspensions of hard spheres did not provide measurements of the three components $(\Sigma_1^p, \Sigma_{22}^p, and \Sigma_{33}^p)$ of the stress tensor Σ^p . Some studies provided measurements of only one of the three components either through direct or indirect measurements. Deboeuf [12] and Deboeuf et al. [13] provided direct measurements of Σ_{33}^p (that was approximated to the particle pressure $\Pi = -(\frac{1}{3})\mathrm{Tr}(\Sigma^p)$) for the shearing flow of monodispersed suspensions in Couette cell geometry. Zarraga et al. [48] reported indirect measurements of the same normal stress component (Σ_{33}^p) by studying the resuspension of a settled suspension in a Couette

flow. Recently, Boyer et al. [4] reported direct measurements of the Σ^p_{22} component of the particle stress tensor. This lack of available measurements for the three components of the particle stress tensor Σ^p has been prevailing since Morris and Boulay [29] reported their work, which forced them to adjust numerically the parameters in the SBM to fit well the experimental data on migration of particles.

In addition to experimental studies, numerical studies for calculating the particle stress components $(\Sigma_{11}^p, \Sigma_{22}^p, \Sigma_{33}^p)$ in monodispersed suspensions are scarce too. Yurkovetsky and Morris [47] performed numerical Stokesian Dynamics (SD) simulations and obtained a particle pressure Π (at high Peclet number) close to that provided by Deboeuf et al. [13]. Using the Force Coupling Method (FCM), Yeo and Maxey [45] calculated the normal stress differences N_1 and N_2 for concentrated monodispersed suspensions of hard spheres. The same workers [46] performed three-dimensional numerical simulations of concentrated suspensions of O(1000) particles in a Couette flow at zero Reynolds number taking into account the wall effects. Their simulations were performed for ϕ between 0.20 and 0.40 and their results agreed well with similar ones reported by Sierou and Brady [43] who adopted the SD approach in their calculations. Both studies indicate that N_1 and N_2 have negative values, and that N_1 is of $O(N_2)$.

Recently, Dbouk et al. [11] reported direct measurements of the normal stress differences N_1 and N_2 in a monodispersed suspension of hard spheres, and determined most of the parameters required by the SBM including the stress tensors Σ , Σ^f , and Σ^p along with their dependence on the volume fraction of particles (ϕ) . Their measurements indicated that N_2 has a negative value, while N_1 has a positive value. This finding is in contradiction with all previous results in the literature. In addition, the ratio $\binom{\Sigma^p}{\Sigma^p_{11}}$ was found to be dependent on the volume fraction ϕ .

The main objective of this work is to implement the SBM within a numerical code capable of predicting simple and general flows of monodispersed concentrated suspensions and to analyze the effects the recently measured parameters [10,11] have on the prediction of particle migration. For that purpose, a two-dimensional solver is developed within the "OpenFOAM®" environment [34] capable of solving the set of conservation equations of the SBM using the finite volume method (FVM) [35]. The FVM is a well-developed numerical approach that guarantees conservation and is widely used for solving fluid flow problems.

In the remainder of this article the conservation equations of the SBM along with its newly adjusted parameters, which are based on the measurements reported by Dbouk et al. [11], are first presented. This is followed by a brief description of the implementation, as a new solver in "OpenFOAM®", of the SBM equations along with its validation by presenting solutions to several concentrated suspensions under simple shearing in one- and two-dimensional domains (i.e. in a rectangular channel and in a wide gap Couette cell). Then, following Miller et al. [28], the code is extended to handle general two-dimensional suspensions for which the flow is no more restricted to be driven by a simple shearing. After validating the general code by generating solutions for neutrally buoyant suspensions in a channel and in a Couette cell, it is extended to account for buoyancy effects. Finally, it is applied to simulate resuspension and mixing of a suspension in a two-dimensional horizontal Couette cell.

2. Shear-induced migration in simple shear flows

2.1. Constitutive modeling (Governing Equations)

This work is concerned with monodispersed non-colloidal suspensions of hard spheres (radius a >1 μ m) that are spread in a

Newtonian Liquid. The flow of these suspensions is viscous (non-inertial) with low particle Reynolds number $\left(Re_p = \frac{\rho_0 \dot{\gamma} a^2}{\eta_0} \ll 1\right)$ and high Peclet number $\left(Pe = \frac{6\pi\eta_0 a^3 \dot{\gamma}}{\kappa T} \gg 1\right)$ to represent a non-Brownian suspension, with $\kappa T(J)$ corresponding to the thermal en-

Brownian suspension, with $\kappa T(J)$ corresponding to the thermal energy, $\dot{\gamma}(s^{-1})$ the shear rate, and η_0 (Pa s) and ρ_0 (kg m⁻³) the dynamic viscosity and density of the Newtonian Liquid phase, respectively.

The suspension is modeled as a continuous medium and the flow is considered to be incompressible and laminar with no external forces. With the above assumptions, the continuity and momentum conservation equations governing the flow in the suspension can be written as

$$\nabla \cdot \boldsymbol{U} = 0, \tag{1}$$

$$\nabla \cdot \mathbf{\Sigma} = \mathbf{0},\tag{2}$$

respectively, where ${\it U}$ is the suspension mean velocity vector, and Σ is the suspension stress tensor. Moreover, a conservation equation for the particle volume fraction (ϕ) can be written as

$$\frac{\partial \phi}{\partial t} + \boldsymbol{U} \cdot \nabla \phi = -\nabla \cdot \boldsymbol{j},\tag{3}$$

where ${\bf j}$ denotes the particle migration flux. So, if one can solve the system of Eqs. (1)–(3), the evolution of the particle phase (ϕ) can be tracked in time (t). There are many models in the literature that provide forms for the particle migration flux ${\bf j}$ such as the diffusion models of Phillips et al. [36], and the flow aligned tensor models of Brady and Morris [5] and Fang et al. [15]. In this work, the Suspension Balance Model (SBM) of Nott and Brady [32] and Morris and Boulay [29] is adopted. This model describes the particle migration flux as the divergence of the particle stress tensor.

2.2. The suspension balance model

The mixture of the two phases (particles + fluid) in this model is considered as a bulk suspension (continuous medium) that obeys the laws of conservation of mass and momentum. Through an averaging procedure, Drew and Lahey [14] obtained the mass conservation equation of the particle phase as

$$\frac{\partial \phi}{\partial t} + \nabla \cdot (\boldsymbol{U}^{p} \phi) = 0, \tag{4}$$

where \mathbf{U}^p is the local velocity of the particle phase.

The momentum conservation of the particle phase at very small Reynolds number with no external forces is given by

$$\nabla \cdot \mathbf{\Sigma}^p + n \langle \mathbf{F}^H \rangle_p = 0, \tag{5}$$

where Σ^p is the particle stress tensor, and $\langle \cdot \rangle_p$ is the average on the particle phase. Moreover, in Eq. (5) n is the number density calculated as

$$n = \frac{3\phi}{4\pi a^3},\tag{6}$$

and \mathbf{F}^H is the hydrodynamic drag force on the particles computed from

$$\mathbf{F}^{H} \simeq -6\pi\eta_{0} a f^{-1}(\phi) (\mathbf{U}^{p} - \mathbf{U}), \tag{7}$$

where $f^{-1}(\phi)$ denotes the mean resistance since $f(\phi)$ is the sedimentation hindrance function that represents the mobility of the particle phase. Miller and Morris [27] used the following form of $f(\phi)$:

$$f(\phi) = \left(1 - \frac{\phi}{\phi_m}\right) (1 - \phi)^{\alpha - 1},\tag{8}$$

where $\alpha \in [2,5]$ is a fitting parameter that depends on the type of particles. Eq. (8) is the functional relationship for $f(\phi)$ adopted here.

However there exists other forms of $f(\phi)$ suggested by other workers such as the one used by Davis and Acrivos [9], and Morris and Boulay [29], which was originally proposed by Richardson and Zaki [39] and is given by

$$f(\phi) = (1 - \phi)^{\alpha},\tag{9}$$

The difference between the two forms is in the dependence of $f(\phi)$ on the maximum packing volume fraction of particles ϕ_m . In order to compare current results with those of Miller and Morris [27], the ϕ_m dependent $f(\phi)$ (Eq. (8)) was adopted. Miller and Morris [27] associated their choice of $f(\phi)$ with the need to ensure that for bounded flows particle migration ceases when the particle concentration approaches maximum packing.

The migration flux j (Eq. (3)) in the SBM is defined as

$$\mathbf{j} = \phi(\mathbf{U}^p - \mathbf{U}),\tag{10}$$

The final form of the flux *i* in the SBM is obtained by combining Eqs. (5), (7) and (10) and is given by

$$\mathbf{j} = \frac{2a^2}{9\eta_0} f(\phi) [\nabla \cdot \mathbf{\Sigma}^p], \tag{11}$$

Therefore, the final form of the particle mass conservation equation (Eq. (3) or (4)) becomes

$$\frac{\partial \phi}{\partial t} + \mathbf{U} \cdot \nabla \phi = -\nabla \cdot \left[\frac{2a^2}{9\eta_0} f(\phi) \nabla \cdot \mathbf{\Sigma}^p \right], \tag{12}$$

As a primary conclusion, the knowledge of Σ^p in the SBM and its variation with ϕ allow predicting the particle migration. In the SBM the total stress Σ in the suspension is decomposed into a fluid phase stress Σ^f , and a particle phase stress Σ^p such that

$$\Sigma = \Sigma^f + \Sigma^p,\tag{13}$$

The fluid phase stress Σ^f is defined as

$$\mathbf{\Sigma}^f = -P_f \mathbf{I} + 2\eta_0 \mathbf{E},\tag{14}$$

where $\mathbf{E} = \frac{1}{2} [\nabla \cdot \mathbf{U} + (\nabla \cdot \mathbf{U})^T]$ is the local rate of strain tensor, and P_f is the pressure of the fluid phase.

It should be noted that the SBM presented here has been revisited recently by Lhuillier [22], and Nott et al. [33]. For them, the particle stress responsible for the migration phenomenon (Eq. (11)) is only due to the direct contact forces between the particles (excluding the hydrodynamic part). However, it is possible that these two models are close at high concentrations where the direct contact between the particles plays the major role. Morris and Boulay [29] suggested the following constitutive law for the particle phase stress for shear flows:

$$\Sigma^p = -\Sigma_{nn}^p + 2\eta_0 \eta_P(\phi) \mathbf{E},\tag{15}$$

where $\Sigma_{nn}^p = \eta_0 \eta_N(\phi) \dot{\gamma} \mathbf{Q}$ is the particle normal stress diagonal tensor, $(2\eta_0\eta_P(\phi)\mathbf{E})$ is the particle shear stress tensor, $\eta_P(\phi) = (\eta_s(\phi))$)-1) is the shear viscosity of the particle phase made dimensionless by the viscosity of the suspending liquid η_0 , $\eta_N(\phi)$ is the normal stress viscosity depending on ϕ , and \bf{Q} is a parametric diagonal tensor of the form

$$\mathbf{Q} = \begin{pmatrix} 1 & 0 & 0 \\ 0 & \lambda_2 & 0 \\ 0 & 0 & \lambda_3 \end{pmatrix},\tag{16}$$

that physically captures the anisotropy of the normal stress of the particle phase. The principal directions of the tensor \mathbf{Q} are those of a viscometric shear flow with 1, 2, and 3 denoting the flow, velocity gradient, and vorticity directions, respectively.

Therefore it is sufficient to provide the parameters $f(\phi), \eta_s, \eta_N, \lambda_2 \left(\lambda_2 = \frac{\Sigma_2^p}{\Sigma_{11}^p}\right)$, and $\lambda_3 \left(\lambda_3 = \frac{\Sigma_3^p}{\Sigma_{11}^p}\right)$ in the SBM (which in turn provides, $\Sigma^f, \Sigma^p, \Sigma$ and j) in order to predict the particle migration in a suspension. The parameters $f(\phi)$ and η_s were modeled in previous studies, whereas η_N , λ_2 , and λ_3 were never measured before. Morris and Boulay [29] used a model for $f(\phi)$ of the form presented in Eq. (9). It should be noted that $f(\phi)$ plays no role in the solutions when seeking the fully-developed flows or steady states in some cases (such as in one dimensional problems). The relative suspension viscosity $\eta_s(\phi)$ was measured experimentally by many rheologists who suggested different functional relationships for its calculation. For example, Maron and Pierce [24] found that $\eta_s(\phi)$ is well modeled via

$$\eta_s(\phi) = \frac{\eta}{\eta_0} = \left(1 - \frac{\phi}{\phi_m}\right)^{-2},$$
(17)

where ϕ_m is the maximum possible packing volume fraction of particles, which depends strongly on the particles shape and interaction. It is measured and found to be between 0.58 and 0.72 for monodispersed suspensions of hard spheres. Morris and Boulay [29] suggested the following relation for $\eta_s(\phi)$:

$$\eta_s(\phi) = \frac{\eta}{\eta_0} \\
= 1 + 2.5 \left(\frac{\phi}{\phi_m}\right) (\phi_m) \left(1 - \frac{\phi}{\phi_m}\right)^{-1} + 0.1 \left(1 - \frac{\phi}{\phi_m}\right)^{-2}, \tag{18}$$

with ϕ_m = 0.68. In addition, they proposed an expression for $\eta_N(\phi)$

$$\eta_N(\phi) = K_N \left(\frac{\phi}{\phi_m}\right)^2 \left(1 - \frac{\phi}{\phi_m}\right)^{-2},\tag{19}$$

where K_N is a fitting parameter that was set at 0.75. Moreover, they adjusted numerically the parameters in the SBM to fit well the experimental data of Phillips et al. [36] for particle migration in a Couette cell, and obtained a constant value of λ_2 equals to 0.8. For λ_3 , they explained how the weakness or the absence of migration observed for the flow of a suspension in a torsional flow between two parallel-disks, implies that λ_3 must be a constant equal to 0.5.

All parameters $\eta_s(\phi)$, $\eta_N(\phi)$, $\lambda_2(\phi)$, and $\lambda_3(\phi)$ can be obtained if and only if $N_1(\phi)$, $N_2(\phi)$, $\eta_s(\phi)$, and all components of the particle stress tensor $\Sigma^p(\phi)$ are known. Reported measurements of $N_1(\phi)$ and $N_2(\phi)$ are scarce and contradictory. In addition, complete measurements of all components of $\Sigma^p(\phi)$ have never been reported due to its complexity, which prevented workers from acquiring a complete set of values based on measurements for the parameters needed in the SBM.

The two normal stress differences in a suspension are defined, based on the isotropy of the fluid stress $\left(\Sigma_{11}^f = \Sigma_{22}^f = \Sigma_{33}^f\right)$, as

$$N_{1} = \Sigma_{11} - \Sigma_{22} = \Sigma_{11}^{p} - \Sigma_{22}^{p} = -\eta_{0}\eta_{N}\dot{\gamma}(1 - \lambda_{2}),$$

$$N_{2} = \Sigma_{22} - \Sigma_{33} = \Sigma_{22}^{p} - \Sigma_{33}^{p} = -\eta_{0}\eta_{N}\dot{\gamma}(\lambda_{2} - \lambda_{3}),$$
(20)

$$N_2 = \Sigma_{22} - \Sigma_{33} = \Sigma_{22}^p - \Sigma_{33}^p = -\eta_0 \eta_N \dot{\gamma} (\lambda_2 - \lambda_3), \tag{21}$$

The definitions of Σ , Σ^f , and Σ^p in Eqs. (13)–(15), in addition to the above definitions in Eqs. (20) and (21), yield a bulk suspension stress Σ in the SBM of the form

$$\Sigma = \Sigma^f + \Sigma^p = -P\mathbf{I} - \eta_0 \eta_N \dot{\gamma} \mathbf{Q} + 2\eta_0 \eta_s \mathbf{E}, \tag{22}$$

where P is the suspension pressure. Thus measuring $N_1(\phi)$, $N_2(\phi)$, $\eta_s(\phi)$, and $\Sigma^p(\phi)$, and using Eqs. (19)–(21) one can get all parameters $(\eta_s(\phi), \eta_N(\phi), \lambda_2(\phi), \text{ and } \lambda_3(\phi))$ needed in the SBM, which are all material functions of a suspension (see [11]).

Recent measurements conducted by the authors of this article [11], indicated that $N_2 < 0$ and $N_1 > 0$. This last finding of a positive N_1 is in contradiction with all previously reported values in the literature. An objective of this paper is to analyze the effect of this positive value for N_1 on the prediction of particle migration via the SBM. In addition, the study Dbouk et al. [11] involved a complete measurement of the particle stress tensor $\Sigma^p(\phi)$ which provided η_N , λ_2 , and λ_3 as functions of the volume fraction of particles ϕ and are given by

$$\eta_N(\phi) = 1.08 \left(\frac{\phi}{\phi_m}\right)^2 \left(1 - \frac{\phi}{\phi_m}\right)^{-2},\tag{23}$$

$$\lambda_2(\phi) = 0.81 \left(\frac{\phi}{\phi_m}\right) + 0.66,$$
(24)

$$\lambda_3(\phi) = -0.0088 \left(\frac{\phi}{\phi_m}\right) + 0.54,$$
(25)

with ϕ_m = 0.58. A higher value of K_N = 1.08 is measured compared to the value of 0.75 reported by Morris and Boulay [29] [Eq. (19)]. Moreover, Eqs. (24) and (25) indicate that λ_2 and λ_3 are functions of the volume fraction ϕ of the particles and not constants as assumed previously (Fig. 1). It should be mentioned here that ϕ_m is extremely difficult to evaluate experimentally and it is a crucial parameter in the rheology of suspension flows. Since everything in the SBM model adopted in the current study scales like the parameter $\left(\frac{\phi}{\phi_m}\right)$, it was decided to keep this representation for all measured parameters of the SBM [i.e. Eqs. (23)–(25)].

3. Numerical procedure

3.1. Numerical technique (the finite volume method)

The coupled system of conservation Eqs. (1)–(3) governing the flow and particle migration in the monodispersed suspension is solved numerically using a collocated finite-volume method. Checkerboard pressure and velocity fields are eliminated through the use of the Rhie-Chow interpolation [38] technique for the calculation of the mass fluxes across the control-volume faces. Pressure-velocity coupling is accomplished through the use of the SIMPLE algorithm [35]. Solutions are obtained by subdividing the physical space into a number of control volumes with grid points placed at their geometric centers (Fig. 2a). The discretized equations are first integrated over a control volume (Fig. 2b) to obtain a discretized description of the conservation law. Then, an interpolation profile is used to reduce the integrated equations to algebraic equations by expressing the variation in the dependent variable and its derivatives in terms of the grid point values. The approximation scheme produces an expression for the face value which is dependent on the nodal values in the vicinity of the face. An algebraic equation is obtained in every control volume with their collection forming a system that is solved iteratively to produce the numerical solution.

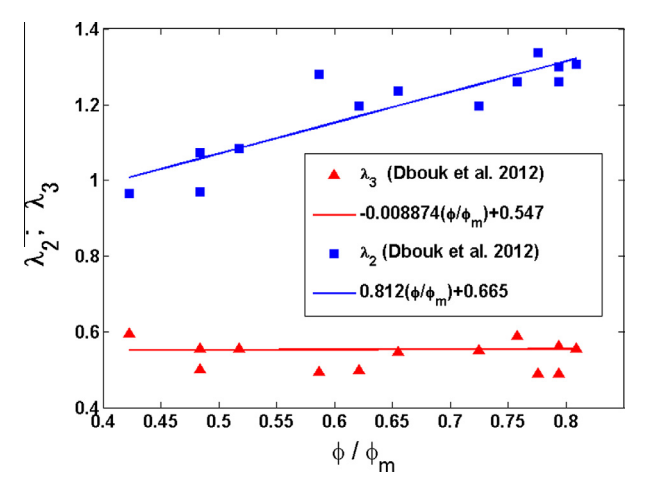


Fig. 1. Variation of $\lambda_2(\phi)$ and $\lambda_3(\phi)$ with ϕ .

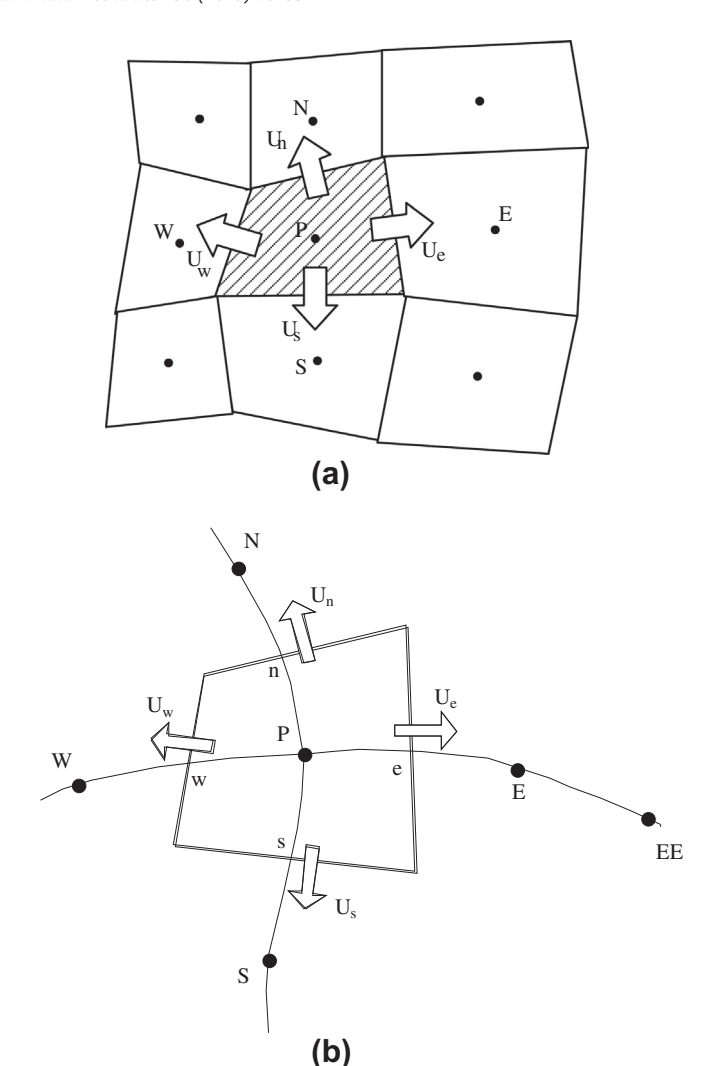


Fig. 2. (a) Space discretization in the control volume method; (b) A typical control volume.

3.2. Implementation of the SBM in "OpenFOAM®"

In this paper, the above described numerical solution algorithm is implemented in the "OpenFOAM®" (Open Field Operation and Manipulation) CFD Toolbox [34], which is an open source software package with a modular code design that allows the user to customize and extend its functionality to develop a suitable solver for the problem under consideration. As mentioned above, the developed code allows solving Eqs. (1) and (2) via the SIMPLE algorithm. The full system of Eqs. (1)-(3) is solved iteratively. The second order Crank-Nicolson [6] transient scheme is used for the discretization of the unsteady term $(\frac{\partial \phi}{\partial t})$ while satisfying the stability criterion (i.e. $Cr < 1, Cr = \frac{\Delta t |U|}{\Delta x}$ is the Courant number). Moreover, the Crank– Nicolson scheme is also adopted for the discretization in time of the diffusion term. In this case physically plausible results are guaranteed by enforcing the term $\eta \frac{\Delta t}{\Delta x^2}$ to be less than 1 (i.e. $\eta \frac{\Delta t}{\Delta x^2} < 1$). Since a fixed grid is used, the value of Δx is chosen and the value of Δt is computed during simulation as the minimum of the two computed values $\left(i.e.\Delta t = MIN\left[\frac{\Delta x^2}{\eta}, \frac{\Delta x}{|U|}\right]\right)$. In space, the Laplacian operator (∇^2), representing the diffusion term, is discretized using the second order Gaussian integration scheme, which is the only choice of discretization available in "OpenFOAM®". The scheme requires the selection of an interpolation procedure for the diffusion coefficient (i.e. η) and the gradient at the control volume faces. In the calculations, a second order unbounded and conservative interpolation procedure is adopted. The discretization of the divergence operator $(\nabla \cdot)$ is performed using the "Gauss" discretization approach, which requires a selection of the interpolation scheme for the dependent field. For that purpose, the bounded first order upwind scheme is used for the calculation of the convective terms, and the second order, unbounded, conservative scheme is employed as an interpolation scheme for the tensorial terms, i.e. $\nabla \cdot \Sigma^p$. Similarly, the "Gauss linear" scheme is used for the interpolation of the gradient terms, i.e. ∇p .

3.3. Validation of implementation in OpenFOAM®

3.3.1. Suspension flow in a rectangular cross-section conduit

Numerical simulations using the developed code in "Open-FOAM®" for the pressure-driven flow of a suspension in a conduit of rectangular cross-section are compared with the numerical results reported by Miller [26] and Miller and Morris [27]. In addition, predictions are compared with the experimental data presented by Lyon and Leal [23] who measured the concentration distribution of the particles using laser-Doppler velocimetry (LDV). In the experiments they used monodispersed spherical polymethyl-methacry-late (PMMA) particles, large enough to neglect Brownian effects, and of diameters between 50 and 100 μ m. Moreover, the particles were immersed in a Newtonian liquid (Triton X-100+ UCON 75-H) of dynamic viscosity η_0 = 0.48 Pa s at 20 °C, and of density ρ_f = 1.19 - g cm⁻³ which was equal to that of the PMMA particles (ρ_p = ρ_f \approx ρ) in order to prevent any sedimentation problems.

The conduit of rectangular cross section was of length L and of width 2H. Consequently, different experimental parameters were chosen in a way to neglect inertia, i.e. $Re_p << 1$ where Re_p is the particles Reynolds number for channel flow defined in a way similar to that for tube flow [23,18] as

$$Re_p = \frac{4}{3} \frac{\rho}{\eta} \frac{a^3}{H^2} U_{max} \tag{26}$$

where U_{max} is the maximum velocity in the suspension and a the averaged particle radius.

The aspect ratio $(\frac{L}{H})$ was chosen in a way to ensure that the measured profiles were at fully developed state. Nott and Brady [32] showed that the profiles are fully developed if

$$\left(\frac{L}{H}\right) \ge \frac{1}{12g(\phi)} \left(\frac{H}{a}\right)^2 \tag{27}$$

where $g(\phi)$ stands for the dependence of the shear-induced diffusion coefficient on the bulk particle concentration. After a good fitting to their experimentally measured diffusion coefficients, Leighton and Acrivos [20,21] and later Chapman [7] found that $g(\phi)$ is best described by the following functional relationship:

$$g(\phi) = \frac{1}{3}\phi^2 \left(1 + \frac{1}{2}e^{8.8\phi}\right) \tag{28}$$

Some zones during the flow may be experiencing a zero shear rate such as at the channel center-line. In this latter situation, the model predicts concentration profiles with a cusp representing a singularity at $\phi = \phi_m$. This singularity is localized in a narrow zone whose size is of the order of magnitude of the particle size, where the description of the suspension as a continuum medium makes no sense any more. In order to eliminate this singularity at the channel center-line, a non-local shear rate $\dot{\gamma}_{NL}$ [27] is defined and added to the local shear rate $\dot{\gamma}$ in Eq. (22), such that

$$\dot{\gamma}_{NL} = a_s \frac{U_{max}}{H} \tag{29}$$

where a_s is equal to 0, ε , or ε^2 and $\varepsilon = \frac{a}{H}$.

The physical domain, schematically depicted in Fig. 3a, is subdivided into 100×20 control volumes. The grid is uniformly distributed in the y direction, but non-uniformly discretized in the x direction with an expansion ratio of 1:50 in the flow direction, in order to better capture the different properties at the inlet of the conduit. The imposed boundary conditions on the conservation equations (Eqs. (1)–(3)) are displayed in Fig. 3b.

In order to check the implementation of the SBM in "Open-FOAM®", the problem was solved using the same model parameters "Case(1)" suggested by Miller and Morris [27], and are given by

Case(1):
$$\eta_N(\phi) = 0.75 \left(\frac{\phi}{\phi_m}\right)^2 \left(1 - \frac{\phi}{\phi_m}\right)^{-2}$$
, $\eta_s = \left(1 - \frac{\phi}{\phi_m}\right)^{-2}$, $f(\phi) = \left(1 - \frac{\phi}{\phi_m}\right) (1 - \phi)^{\alpha - 1}$, $\phi_m = 0.68$, $\alpha = 4$, $\lambda_2 = 0.8$, $\lambda_3 = 0.5$, and $a_s = \varepsilon$.

Steady state fully developed particle concentration profiles are compared in Fig. 3 with similar results reported by Miller and Morris [27] for a conduit with $\frac{H}{a}=18$. Fig. 4a–c compare ϕ profiles at $\frac{x}{L}=0.85$ obtained with suspensions having initial concentrations with values of $\phi_b=0.30$, 0.40, and 0.50, respectively. Fig. 4d compares the variation of ϕ for the various initial bulk concentrations along the centerline of the conduit. As shown, current numerical results are in good agreement with those reported by Miller and Morris [27] validating the implementation of the SBM in "Open-FOAM®". By comparing the numerical predictions obtained using the SBM with the experimental data of Lyon and Leal [23] (Fig. 4a–c), a large difference near the walls is seen. This difference is attributed to the indirect measurements of the volume fraction (ϕ) values using the LDV.

It may be of interest to mention that the calculation time for the cases presented in this part varied between 1 and 30 min (1 min $\leq t_{calc} \leq$ 30 min) with a CPU of 1 GHz. The higher the ϕ_b value was, the greater the computational time became, due to the need to decrease the time step (δt_{calc}).

For the same problem, solutions are obtained using values for the parameters of the SBM obtained from the measurements performed by the authors "Case(2)" [11], which are given by

Case(2):
$$\eta_N(\phi) = 1.08 \left(\frac{\phi}{\phi_m}\right)^2 \left(1 - \frac{\phi}{\phi_m}\right)^{-2}$$
, $\eta_s = \left(1 - \frac{\phi}{\phi_m}\right)^{-2}$, $f(\phi) = \left(1 - \frac{\phi}{\phi_m}\right)(1 - \phi)^{\alpha - 1}$, $\phi_m = 0.68$, $\alpha = 4$, $\lambda_2 = 0.81 \left(\frac{\phi}{\phi_m}\right) + 0.66$, $\lambda_3 = -0.0088 \left(\frac{\phi}{\phi_m}\right) + 0.54$, and $a_s = \varepsilon$.

Profiles presented in Fig. 5 indicate that there is little difference between the results in Case(1) (proposed SBM parameters) and that in Case(2) (measured SBM parameters) for the predictions of the particle steady concentration profiles across the channel (Fig. 5a–c). Nevertheless, a small difference is observed in the predictions of the particle steady concentration profiles along the centerline of the channel (Fig. 5d), especially at low values of the bulk volume fraction in the inlet region (x/L < 0.2). The new values of parameters [Case(2)] tend to enlarge more the centerline steady concentration region.

The effects of using the two different forms of $f(\phi)$ given by Eqs. (8) and (9) on particle migration in the channel are studied by using the following SBM parameters [Case (2')] and comparing results to those obtained previously [Case(2)]:

Case(2'):
$$\eta_N(\phi) = 1.08 \left(\frac{\phi}{\phi_m}\right)^2 \left(1 - \frac{\phi}{\phi_m}\right)^{-2}$$
, $\eta_s = \left(1 - \frac{\phi}{\phi_m}\right)^{-2}$, $f(\phi) = (1 - \phi)^{\alpha}$, $\phi_m = 0.68$, $\alpha = 4$, $\lambda_2 = 0.81 \left(\frac{\phi}{\phi_m}\right) + 0.66$, $\lambda_3 = -0.0088 \left(\frac{\phi}{\phi_m}\right) + 0.54$, and $a_s = \varepsilon$.

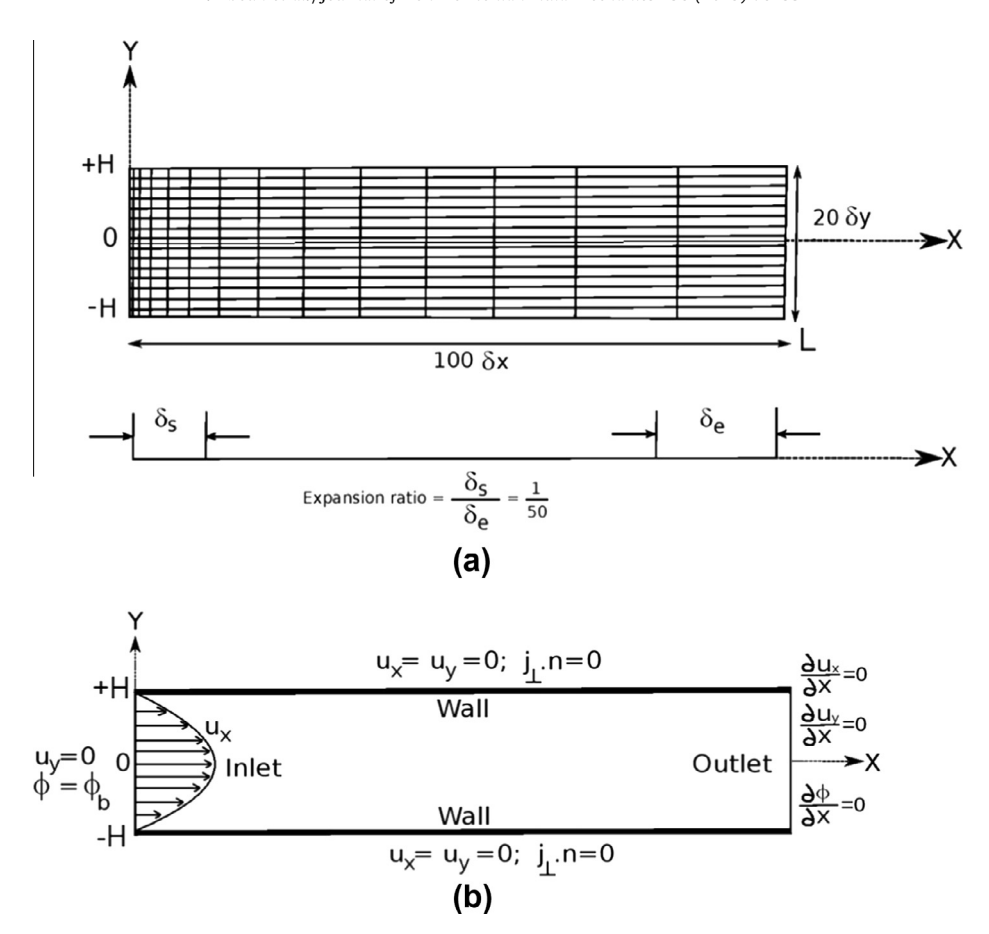


Fig. 3. (a) Grid system used in the two-dimensional channel of rectangular cross-section; (b) Boundary conditions used in the computations.

Results presented in Fig. 6a–c show that the form of $f(\phi)$ has no effect on the particle steady concentration profiles across the channel for all values of ϕ_b considered (i.e. $0.3 \le \phi_b \le 0.5$). Nevertheless, a small difference is observed in the predictions of the particle steady concentration profiles along the centerline of the channel (Fig. 6d), especially in the inlet region (x/L < 0.2).

One may ask if a comparison when ϕ reaches ϕ_m (in the absence of any experimental data) could not discriminate between the different model parameters $(f(\phi), \eta_s, \eta_N, \lambda_2\left(\lambda_2 = \frac{\Sigma_{22}^p}{\Sigma_{11}^p}\right)$, and $\lambda_3\left(\lambda_3 = \frac{\Sigma_{22}^p}{\Sigma_{11}^p}\right)$. In fact, as was mentioned previously in Dbouk et al. [11], it was extremely difficult to extract trusted measurements when ϕ is greater than $0.81\phi_m$. Accordingly, it would be unsafe to extrapolate these experimental results for higher concentrations. For that reason, future experiments are certainly needed to better capture the SBM parameters at high concentrations, with their measurements conducted alongside the evolution of migration.

3.3.2. Suspension flow in a cylindrical Couette cell

As a second check for the correct implementation of the SBM in "OpenFOAM®", the flow of a suspension in a cylindrical Couette cell is considered. The physical situation is schematically depicted in Fig. 7 and represents the flow of a suspension between two concentric cylinders, where the inner cylinder is rotating with an angular velocity Ω , while the outer cylinder is stationary. Initially, the suspension has a uniform distribution of particles in the radial direction between the two cylinders with $\phi = \phi_b$. During the flow, it is observed that the particles migrate toward the outer cylinder.

The modeled situation is the one experimentally studied by Phillips et al. [36] in which the inner and outer radii of the Couette cell are 0.64 cm and 2.38 cm, respectively, the cavity length is 25 cm, and the suspension is composed of PMMA spheres of mean diameter $2a = 675 \, \mu \text{m}$, suspended in a Newtonian liquid mixture of dynamic viscosity $\eta_0 = 9.45 \, \text{Pa s}$ at $23.15 \, ^{\circ}\text{C}$, and of density $\rho_f = \rho_p = \rho = 1.182 \, \text{g cm}^{-3}$. Using the NMR technique, they were able to perform direct measurements of the volume fraction of particles in the gap between the cylinders.

In the numerical simulations, the cylinders are assumed to be of infinite length and body forces to be negligible, thus reducing the problem to a one-dimensional one with variation occurring in the radial direction. The wedge-type geometry defined in "Open-FOAM®" was used due to the axi-symmetric geometry of the problem. The domain, shown in Fig. 7a, is subdivided into 20 control volumes of equal size, while the boundary conditions used are displayed in Fig. 7b. It should be mentioned here that for the flow in a Couette cell geometry the orientation in the code of the tensor **Q** (Eq. (16)) is given by

$$\mathbf{Q} = \begin{pmatrix} \lambda_2 & 0 & 0 \\ 0 & 1 & 0 \\ 0 & 0 & \lambda_3 \end{pmatrix} (\theta, r, z), \tag{30}$$

This is required in order to respect the orientation of the principal directions in the SBM for simple shear flows (i.e. 1, 2, and 3 denoting the flow, velocity gradient, and vorticity directions, respectively).

For direct comparison of results, the problem was first solved using the same model parameters suggested by Morris and Boulay [29] "Case(1A)", and are given by

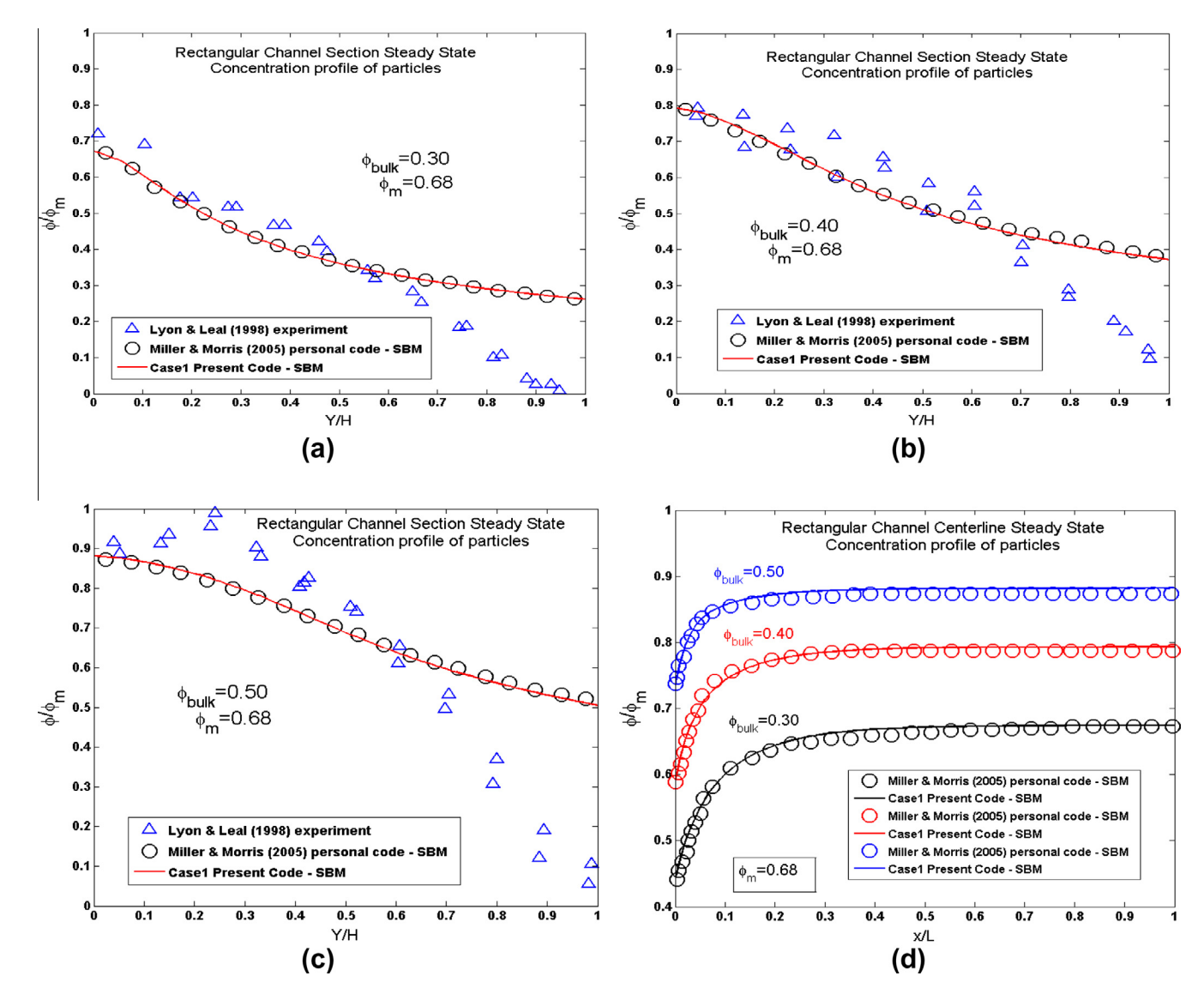


Fig. 4. Comparison of steady state concentration profiles at $\frac{x}{L} = 0.85$ (a)–(c) obtained numerically using the SBM [Case(1)] with similar experimental data and numerical results reported in the literature for particle migration in a conduit of rectangular cross-section for ϕ_b values of (a) 0.3, (b) 0.5, and (c), 0.5; (d) Comparison of numerical [Case(1)] steady state concentration profiles along the center line of the channel with similar numerical results reported in the literature for the various values of ϕ_b .

Case(1A):
$$\eta_N(\phi) = 0.75 \left(\frac{\phi}{\phi_m}\right)^2 \left(1 - \frac{\phi}{\phi_m}\right)^{-2}$$
, $\eta_s(\phi) = 1 + 2.5 \left(\frac{\phi}{\phi_m}\right) (\phi_m)$ $\left(1 - \frac{\phi}{\phi_m}\right)^{-1} + 0.1 \left(1 - \frac{\phi}{\phi_m}\right)^{-2}$, $f(\phi) = (1 - \phi)^{\alpha}$, $\phi_m = 0.68$, $\alpha = 4$, $\lambda_2 = 0.8$, $\lambda_3 = 0.5$, and $a_s = 0$.

It is to be noted here that since the flow is one-dimensional, λ_3 has no role to play and has no effect on the results. Transient and steady state profiles of the particles volume fraction in a suspension with bulk concentration of value ϕ_b = 0.55 and a particle of size $\frac{a}{R_{out}} = 0.0143$ are depicted in Fig. 8. Fig. 8a compares the particle distribution profiles after 200 revolutions of the inner cylinder, while profiles in Fig. 8b are after the lapse of 12,000 revolutions. As shown, the SBM predicts the correct direction of migration of particles toward the outer cylinder, and quantifies well the particles distribution in the gap. Results generated in this work using "OpenFOAM®" are closer to the experimental data of Phillips et al. [36] than the one-dimensional numerical simulations reported by Morris and Boulay [29]. The small differences between current numerical profiles and those obtained by Morris and Boulay [29], may be due to different interpolation schemes as the number of grid points used in the numerical solution is small.

By solving the conservation equations of mass and momentum in a cylindrical coordinate system, a semi-analytical solution for the concentration of particles at steady state is obtained as [29]

$$\frac{\eta_N(\phi)}{\eta_S(\phi)} = q(\phi) = A_c r^{\frac{1+\lambda_2}{\lambda_2}},\tag{31}$$

where A_c is a constant that should be determined by requiring $\phi(r)$ to average to the imposed bulk concentration such that

$$\phi_b \pi \left(R_o^2 - R_i^2 \right) = \int_{R_i}^{R_o} \phi(r) 2\pi r dr.$$
 (32)

The solution is semi-analytic as it requires knowledge of the function $q(\phi)$ in order to calculate ϕ . In this work, the suggested expressions for $\eta_N(\phi)$ and $\eta_S(\phi)$ [Case(1A)] are used to find the expression for $q(\phi)$.

The steady state concentration profiles shown in Fig. 8c indicate that numerical results obtained with "OpenFOAM®" fall on top of the semi-analytic profile generated using Eqs. (31) and (32), and are in excellent agreement with the semi-analytic profile reported by Morris and Boulay [29] and the measured data of Phillips et al. [36].

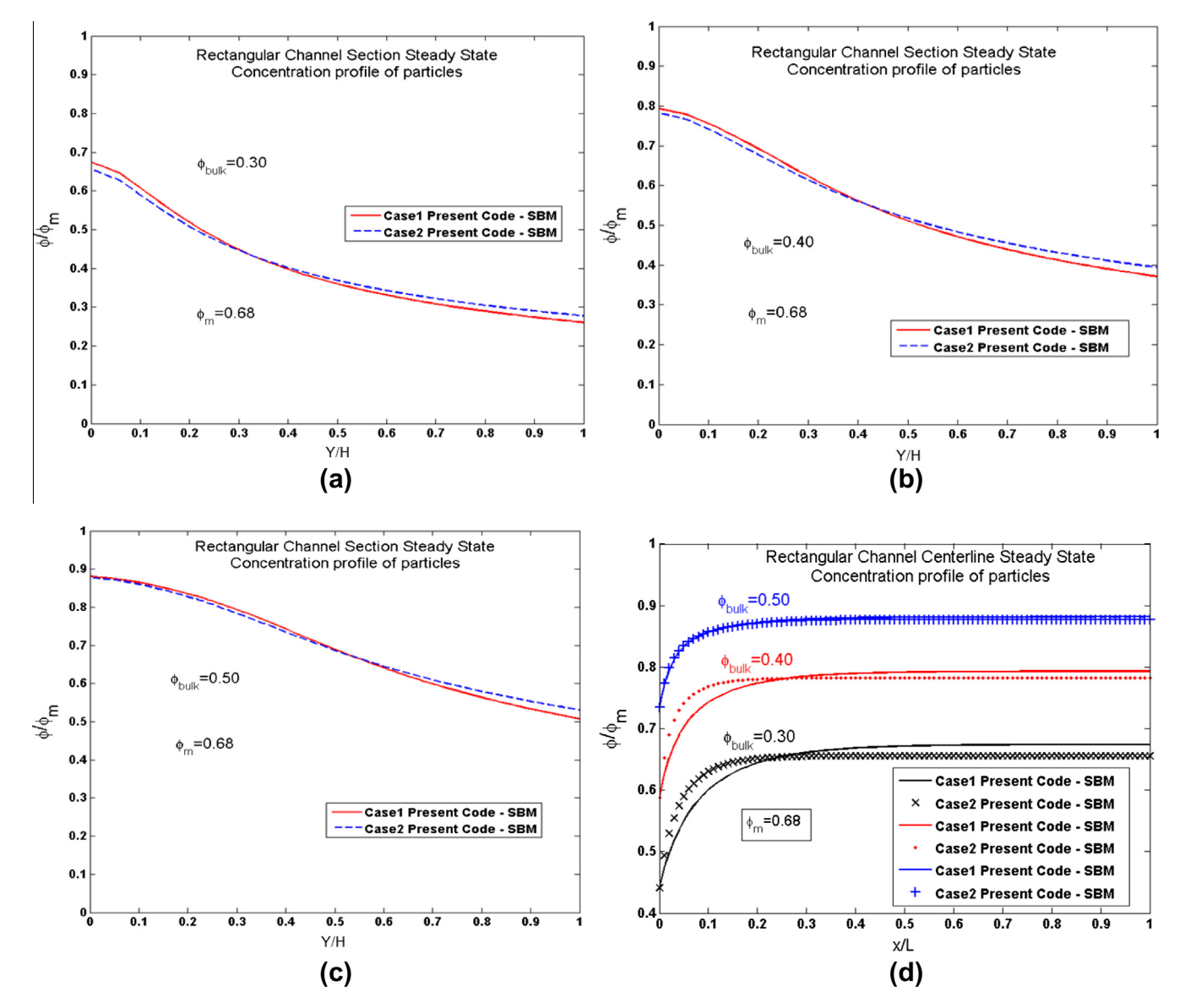


Fig. 5. Comparison of steady state concentration profiles at $\frac{x}{L} = 0.85$ (a)–(c) obtained numerically using the SBM [Case(1)] and modified SBM [Case(2)] for particle migration in a conduit of rectangular cross-section for ϕ_b values of (a) 0.3, (b) 0.4, and (c), 0.5; (d) Comparison of steady state concentration profiles along the center line of the channel obtained with the SBM [Case(1)] and modified SBM [Case(2)] for the various values of ϕ_b .

The values of the parameters in the SBM were changed here to the experimentally measured values [11] and solutions were generated using two different functional relationships for $\eta_s(\phi)$ suggested by Maron and Pierce [24] and Morris and Boulay [29] and resulting in two sets of coefficients that are designated by "Case(2A)" and "Case(2B)", respectively, and are given by

Case(2A):
$$\eta_N(\phi) = 1.08 \left(\frac{\phi}{\phi_m}\right)^2 \left(1 - \frac{\phi}{\phi_m}\right)^{-2}$$
, $\eta_s(\phi) = \left(1 - \frac{\phi}{\phi_m}\right)^{-2}$, $f(\phi) = \left(1 - \frac{\phi}{\phi_m}\right) (1 - \phi)^{\alpha - 1}$, $\phi_m = 0.68$, $\alpha = 4$, $\lambda_2 = 0.81 \left(\frac{\phi}{\phi_m}\right) + 0.66$, $\lambda_3 = -0.0088 \left(\frac{\phi}{\phi_m}\right) + 0.54$, and $a_s = 0$. Case(2B): $\eta_N(\phi) = 1.08 \left(\frac{\phi}{\phi_m}\right)^2 \left(1 - \frac{\phi}{\phi_m}\right)^{-2}$, $\eta_s(\phi) = 1 + 2.5 \left(\frac{\phi}{\phi_m}\right) (\phi_m) \left(1 - \frac{\phi}{\phi_m}\right)^{-1} + 0.1 \left(1 - \frac{\phi}{\phi_m}\right)^{-2}$, $f(\phi) = \left(1 - \frac{\phi}{\phi_m}\right) (1 - \phi)^{\alpha - 1}$, $\phi_m = 0.68$, $\alpha = 4$, $\lambda_2 = 0.81 \left(\frac{\phi}{\phi_m}\right) + 0.66$, $\lambda_3 = -0.0088 \left(\frac{\phi}{\phi_m}\right) + 0.54$, and $a_s = 0$.

Fig. 9a and b compare the profiles for $q(\phi)=\frac{\eta_N(\phi)}{\eta_S(\phi)}$ and ϕ , respectively, for Case(1A), Case(2A), and Case(2B). The profile for $q(\phi)$ used by Morris and Boulay [29] falls in between the profiles obtained with the current measurements [11]. The use of the latest data for $\eta_N(\phi)$ shows acceptable predictions for the particle migration at 200 revolutions. Nevertheless, these predictions deviate more and more away from the experimental profiles provided by Phillips et al. [36] as the inner cylinder reaches 12,000 revolutions. Here, one should not forget that the bulk concentration is $\phi_b = 0.55$ and the maximum packing volume fraction is ϕ_m = 0.68. However, in the conducted experiments, the range of the bulk concentration of particles for which the measurements were taken was less than 0.47 (ϕ_b < 0.47), where after constituting the equation for $\eta_s(\phi)$, resulted in a value for $\phi_m \approx 0.58$. Moreover, Fig. 9 shows clearly that the form of the suspension viscosity $\eta_S(\phi)$ affects more the prediction of migration in a Couette cell gap than the normal suspension viscosity $\eta_N(\phi)$. This becomes more apparent as steady state is approached after many revolutions of the inner cylinder.

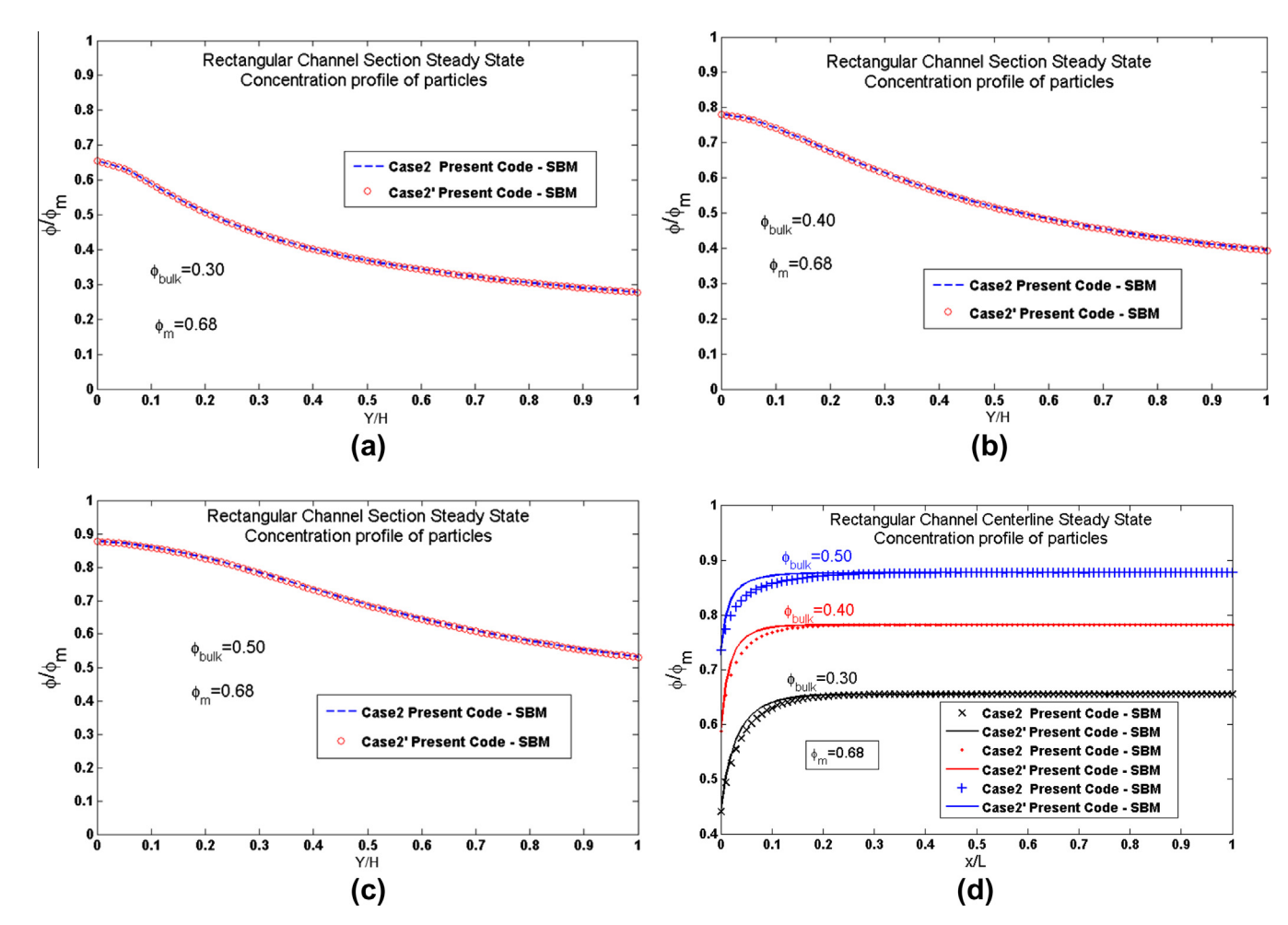


Fig. 6. Comparison of steady state concentration profiles at $\frac{x}{L} = 0.85$ (a-c) obtained numerically using the modified SBM [Case(2)] and modified SBM [Case(2')] for particle migration in a conduit of rectangular cross-section for ϕ_b values of (a) 0.3, (b) 0.4, and (c), 0.5; (d) Comparison of steady state concentration profiles along the center line of the channel obtained with the modified SBM [Case(2)] and modified SBM [Case(2)] for the various values of ϕ_b .

4. The SBM for general flows

The formulation of the SBM presented so far is applicable to cases of simple shear flows of non-Brownian suspensions. This limitation on the use of the model is due to its formulation in a coordinate system that requires its axes to be aligned with the flow, velocity gradient, and vorticity directions. If the model is to be used for two-phase suspensions in general geometries, where the flow is not necessarily of the simple shear type, it requires modifications. Following the efforts of Miller et al. [28], the process of developing a two-dimensional frame-invariant version of the modified SBM presented in the previous sections, which is valid for modeling suspension flows in general two-dimensional geometries, is described next

4.1. Frame-invariant suspension kinematics

The suspension flow kinematics represents the local motion or behavior that a local zone of the suspension (fluid-particles) may undergo. It is the zone where the particles immersed in the fluid may be going away from each other, approaching each other, colliding, or even rolling over each other aligning in a preferred position by the flow between both the compression and the tension axes, as schematically depicted in Fig. 10. Therefore, in the general flow of a suspension, the local kinematics can vary between pure extension and solid-body rotation, with simple shear representing

an equal balance between them. Brady and Morris [5] and Morris and Katyal [31] related the appearance of shear-induced normal stresses in suspensions to the breaking of fore-aft symmetry of the pair-particle microstructure. Since this symmetry is expressed in terms of the driving flow, it is essential to relate the particle stress Σ^p to the local kinematics of the flow. The local kinematics between shearing and extending suspension flows is presented here following the work of Miller et al. [28] that was inspired by the work of Schunk and Scriven [42] and Bird et al. [1] on polymers. The basic idea is to develop an anisotropic particle stress $\Sigma^{p'}$ using the local kinematics of the flow.

4.1.1. Kinematic ratio

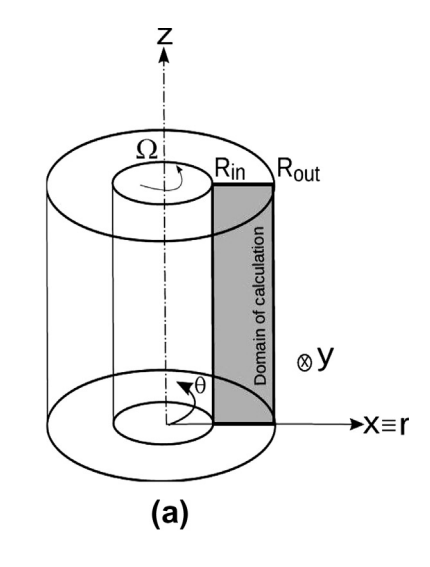
The local kinematics of the suspension is characterized by the local material deformation rate $(\dot{\gamma})$ and the relative rotation (ω_{rel}) defined as

$$\dot{\gamma} = \sqrt{2\mathbf{E} : \mathbf{E}},\tag{33}$$

$$\boldsymbol{\omega}_{rel} = \frac{\omega}{2} - \boldsymbol{W},\tag{34}$$

where ${\bf E}$ is the rate of strain tensor, ${\bf \omega}$ the local vorticity (${\bf \omega} = \nabla \times {\bf U}$) and $(\frac{\omega}{2})$ the local angular velocity of a fluid element, and ${\bf W}$ the local rotation of the axes of the rate of strain given by

$$\boldsymbol{W} = \boldsymbol{e}_i \times \left[\frac{\partial e_i}{\partial t} + \boldsymbol{U} \cdot \nabla \boldsymbol{e}_i \right], \tag{35}$$



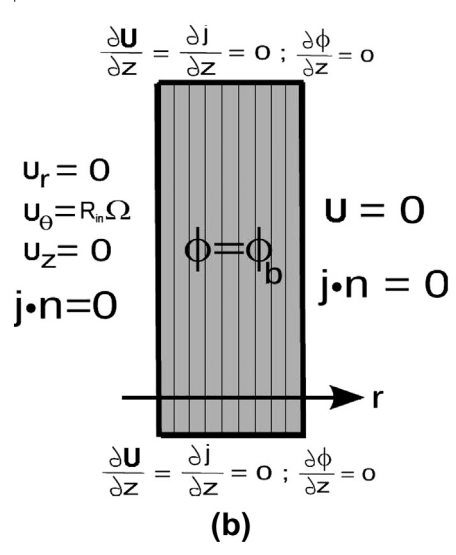


Fig. 7. (a) Schematic of the physical domain for the suspension flow in a Coutte cell problem; (b) computational domain and boundary conditions used in the numerical solution of the suspension flow in a Coutte cell problem.

In Eq. (35) e_i is an eigenvector corresponding to an eigenvalue Λ_i of E satisfying

$$(\mathbf{E} - \mathbf{\Lambda}_i) \cdot \mathbf{e}_i = 0, \tag{36}$$

Since both ω_{rel} and \boldsymbol{W} are calculated using the same frame of reference, their difference (ω_{rel}) produces a frame invariant measure of rotation [26]. Moreover, as the interest here is in quasi-stationary flows, the term $\frac{\partial e_l}{\partial t}$ in Eq. (35) is neglected. Furthermore, these two local kinematic effects $(\dot{\gamma}$ and $\omega_{rel})$ are accounted for through a single kinematic ratio $(\hat{\rho}_k)$, which, following Ryssel and Brunn [40], is defined as

$$\hat{\rho}_{k} = \frac{2|\omega_{rel}|}{(\dot{\gamma}/2) + |\omega_{rel}|} \tag{37}$$

Eq. (37) indicates that $\hat{\rho}_k$ varies between 0 and 2 according to the flow local kinematic state. For a flow in pure extension $\hat{\rho}_k = 0(|\omega_{rel}| = 0)$, in simple shear $\hat{\rho}_k = 1\left(|\omega_{rel}| = \frac{\hat{\gamma}}{2}\right)$, and in solid body rotation $\hat{\rho}_k = 2(\hat{\gamma} = 0)$.

4.1.2. Compression-tension coordinates and transition matrix

To represent the stress in terms of local kinematics in twodimensional situations, the eigenvectors \mathbf{e}_i are defined as the principal axes of the rate of the strain tensor \mathbf{E} , where the subscript $i \equiv t$ stands for the tension axis corresponding to the positive eigenvalue of $E(\Lambda_{i \equiv t} > 0)$, and $i \equiv c$ for the compression axis corresponding to the negative eigenvalue of $E(\Lambda_{i \equiv t} < 0)$ as shown in Fig. 11a and b. Consequently, the transformation relation that maps the general Cartesian system (e_x, e_y, e_z) to the local frame of reference (e_t, e_c, e_z) is given by the transition Matrix T_m as

$$\boldsymbol{T}_{m} = \begin{bmatrix} \boldsymbol{e}_{t} \begin{pmatrix} e_{t1} \\ e_{t2} \\ 0 \end{pmatrix} | \boldsymbol{e}_{c} \begin{pmatrix} e_{c1} \\ e_{c2} \\ 0 \end{pmatrix} | \boldsymbol{e}_{z} \begin{pmatrix} 0 \\ 0 \\ 1 \end{pmatrix} \end{bmatrix}, \tag{38}$$

with the inverse matrix $(T_m)^{-1}$, which is equal to its transpose $(T_m)^T$ due to the symmetry of E, mapping the local frame of reference $(e_t, -e_c, e_z)$ back to the Cartesian system (e_x, e_y, e_z) .

4.2. Anisotropic Particle Stress ($\Sigma^{p'}$) in the SBM

The Σ_{nn}^p tensor of the SBM [Eq. (15)] valid for simple shear flows only, is set up in a two-dimensional compression–tension coordinate system (\mathbf{e}_t , \mathbf{e}_c , \mathbf{e}_z), and extended to a new anisotropic tensor Σ^p dependent on $\hat{\rho}_k$ and valid for general flows. This extension provides a frame of reference independent of the two-dimensional geometry of the flow, but strongly dependent on the local kinematic state of the suspension flow. The extension of Σ_{nn}^p to $\Sigma^{p'}$ is done as follows:

$$\frac{\Sigma^{p}}{\boldsymbol{e}_{t}, \boldsymbol{e}_{c}, \boldsymbol{e}_{z}} = \begin{bmatrix}
\frac{\Sigma_{11}^{p} + \Sigma_{22}^{p}}{2} & \frac{N_{1}}{2} & 0\\ \frac{N_{1}}{2} & \frac{\Sigma_{11}^{p} + \Sigma_{22}^{p}}{2} & 0\\ 0 & 0 & \Sigma_{22}^{p}
\end{bmatrix},$$
(40)

$$\frac{\boldsymbol{\Sigma}^{p'}}{\boldsymbol{e}_{t},\boldsymbol{e}_{c},\boldsymbol{e}_{z}} = \begin{bmatrix}
\frac{\Sigma_{11}^{p} + \Sigma_{22}^{p}}{2} \cdot B_{t}(\hat{\rho}_{k}) & \frac{N_{1}}{2} \cdot C(\hat{\rho}_{k}) & 0 \\
\frac{N_{1}}{2} \cdot C(\hat{\rho}_{k}) & \frac{\Sigma_{11}^{p} + \Sigma_{22}^{p}}{2} \cdot B_{c}(\hat{\rho}_{k}) & 0 \\
0 & 0 & \Sigma_{33}^{p}
\end{bmatrix},$$
(41)

In Eq. (41), $B_t(\hat{\rho}_k)$ and $B_c(\hat{\rho}_k)$ are the functions that weight the particle normal stress in the tension and compression directions, respectively, with Σ_{33}^p being the stress component in the out-of-plane direction. Moreover, $C(\hat{\rho}_k)$ corresponds to the tangential stress weighting function. The values for $B_t(\hat{\rho}_k)$, $B_c(\hat{\rho}_k)$, and $C(\hat{\rho}_k)$ adopted in this work are the ones suggested by Miller et al. [28] and are summarized in Fig. 11c. The physical explanation behind the choice of the values for these weighting functions and their variation with $\hat{\rho}_k$ is as follows:

- **Simple shear flow**: In a simple shear flow situation, $\hat{\rho}_k = 1$ and the values are set to $B_t = B_c = C = 1$ such that the tensor $\Sigma^{p'}$ after being transformed to the Cartesian coordinate system goes back to be equal to Σ^p_{nn} .
- **Pure extension**: In this case B_t is set to zero since during a pure extension [see Fig. 11a], the particles are far away from each other and the normal stress along the extensional axis is almost zero. Nonetheless C, which represents the tangential stress, should also be set to zero.
- **Rotation**: When $\hat{\rho}_k > 1$. it is assumed that rotation plays no role and all weighting coefficients are set to 1 $(B_t = B_c = C = 1)$.
- **Combination of shear and extension**: For $0 < \hat{\rho}_k < 1$, the weighing functions B_t , B_c , and C are linearly interpolated to account for the local kinematics between the compression and tension axes (Fig. 11c).

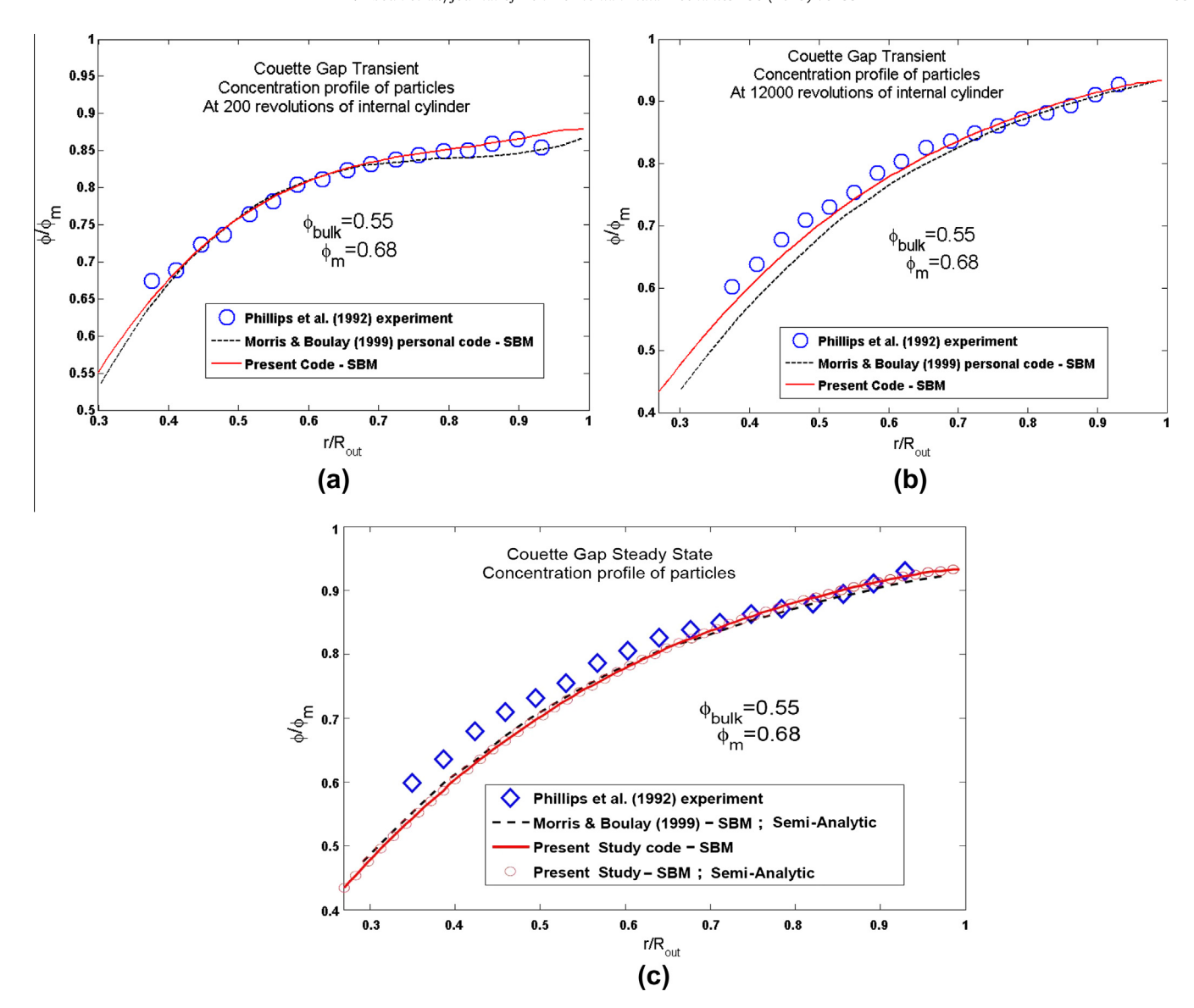


Fig. 8. Comparison of concentration profiles obtained numerically using the SBM [Case(1)] with similar numerical and experimental results reported in the literature for particle migration in a Couette cell geometry at (a) 200 revolutions, (b) 12,000 revolutions, and (c) steady state.

Finally, it should be noted that the tensor $\Sigma^{p'}$ is mapped back from the local coordinate system to the general Cartesian coordinate system using the transformation matrix T_m such that

$$\frac{\boldsymbol{\Sigma}^{p\prime}}{\boldsymbol{e}_{x},\boldsymbol{e}_{y},\boldsymbol{e}_{z}} = \leftarrow \boldsymbol{T}_{m} \cdot \frac{\boldsymbol{\Sigma}^{p\prime}}{\boldsymbol{e}_{t},\boldsymbol{e}_{c},\boldsymbol{e}_{z}} \cdot \boldsymbol{T}_{m}^{-1}, \tag{42}$$

4.3. Validation

The above-described frame-Invariant two-dimensional SBM was implemented in "OpenFOAM®". The validity of the code is established in this section by comparing results generated using the frame-invariant code to previous results obtained with the frame-dependent code for the suspension flows in a wide gap Couette cell [36] and a channel of rectangular cross-section [23].

Note that, even though the flow of the suspensions in these geometries is of the simple shear type, the intention is simply to compare results in order to validate the new code for the transformation of the tensor $\Sigma^{p'}$ [Eq. (42)] between the local $(\mathbf{e}_t, \mathbf{e}_c, \mathbf{e}_z)$ and the general $(\mathbf{e}_x, \mathbf{e}_v, \mathbf{e}_z)$ coordinate systems. The comparison of results

is displayed in Fig. 12a for the suspension flow in a rectangular channel and in Fig. 12b for the flow in a wide gap Couette cell. As shown in both figures, results are on top of each other indicating correct implementation of the frame-invariant model.

5. The SBM extended to include buoyancy effects

5.1. Conservation equations for buoyant suspensions

Developments in the previous sections dealt with the general flow of neutrally buoyant suspensions for which the particle and fluid phases are of equal densities. The question arises regarding the effects the difference in density might have on particle migration in buoyant suspensions ($\rho_p \neq \rho_f$). Such situations occur, for example, during viscous resuspension when a fluid flows past an initially settled bed of heavy particles, to disturb and resuspend the sediment layer. The problem was first reported by Gadala-Maria [16] and later investigated experimentally and numerically by Leighton and Acrivos [19], Leighton and Acrivos [20,21], Schaflinger et al. [41], Rao et al. [37]. To account for that phenomenon,

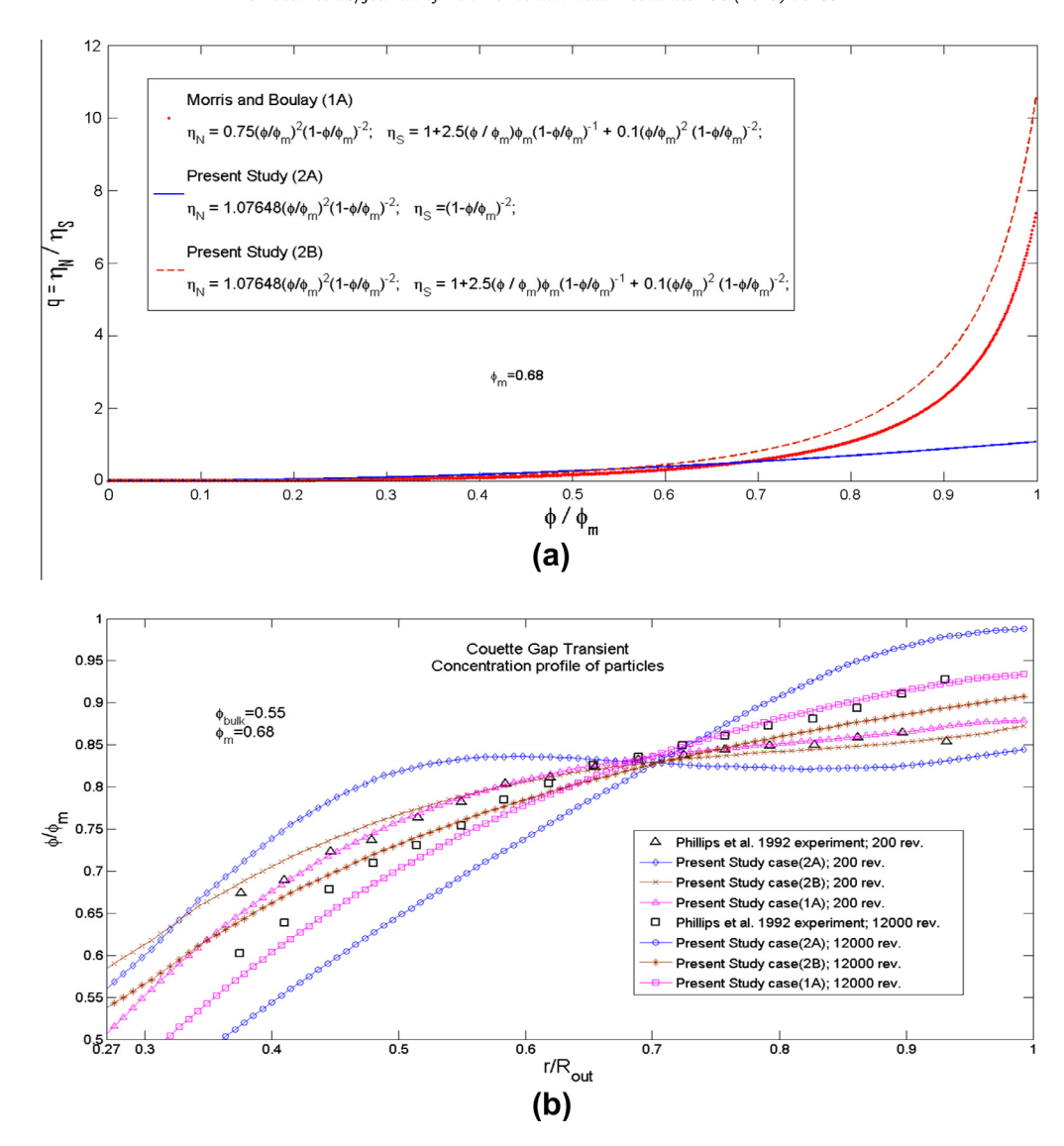


Fig. 9. (a) Comparison of $q(\phi)$ profiles obtained using different functional relationships of η_N ; (b) comparison of concentration profiles at 200 and 12,000 revolutions obtained numerically using different values of the SBM parameters [Case(1A), Case(2A), and Case(2B)] with experimental values reported in the literature for particle migration in a Couette cell geometry.

which is the true general case in nature, buoyancy effects should be included in the transport conservation equations [Eqs. (1)–(3)] of the SBM.

Let the particle and fluid phase densities be designated by ρ_p^i and ρ_p^i , respectively. Based on the particle phase volume fraction (ϕ) , the mixture density ρ can be written as

$$\rho = \rho_p + \rho_f \text{ with } \rho_p = \phi \rho_p^i \text{ and } \rho_f = (1 - \phi) \rho_f^i \tag{43}$$

The suspension mass and momentum conservation equations become, respectively,

$$\nabla \cdot \boldsymbol{U} = 0, \tag{44}$$

and

$$\nabla \cdot \mathbf{\Sigma} + \Delta \rho^i \mathbf{g} \phi = 0, \tag{45}$$

where

$$\Delta \rho^i = \rho_p^i - \rho_f^i, \tag{46}$$

is the difference in material densities, and \boldsymbol{g} is the gravitational acceleration. Moreover, inclusion of buoyancy effects in the transport equation of the particle phase results in

$$\frac{\partial \phi}{\partial t} + \boldsymbol{U} \cdot \nabla \phi = -\nabla \cdot \boldsymbol{j}_{total}, \tag{47}$$

with

$$\boldsymbol{j}_{total} = \boldsymbol{j} + \boldsymbol{j}_{g}, \tag{48}$$

where \mathbf{j} is the migration flux defined previously in Eq. (11) and \mathbf{j}_g the migration flux due to buoyancy, which is modeled as a Stokes single particle velocity \mathbf{v}_{stokes} multiplying a hindered settling function $f(\phi)$, given by

$$\mathbf{j}_{g} = f(\phi) \mathbf{v}_{\text{stokes}} \phi, \tag{49}$$

 $f(\phi)$ is the same hindrance function defined previously in Eq. (8), and \mathbf{v}_{stokes} is the Stokes velocity written in terms of the particle radius (a), the density difference $(\Delta \rho^i)$, the gravitational acceleration, and the viscosity of the pure fluid as

$$\pmb{v}_{\text{stokes}} = \frac{2}{9} \frac{a^2 \Delta \rho^i g}{\eta_0}, \tag{51}$$

To this end, the code developed for the frame-invariant model presented in the previous section was extended to include buoyancy effects following the changes described above.

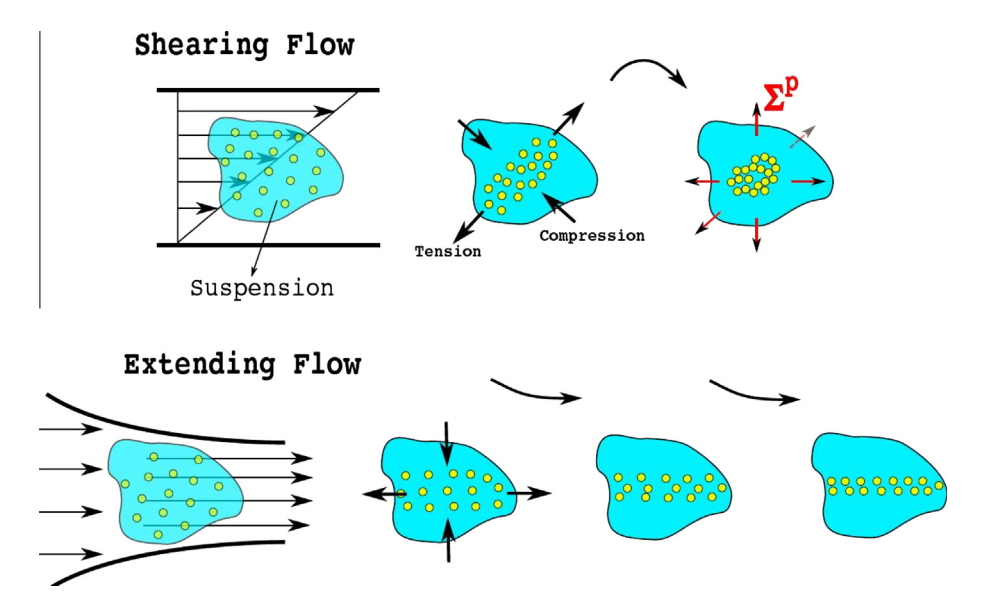


Fig. 10. Different types of flow in suspensions varying between shearing and extending.

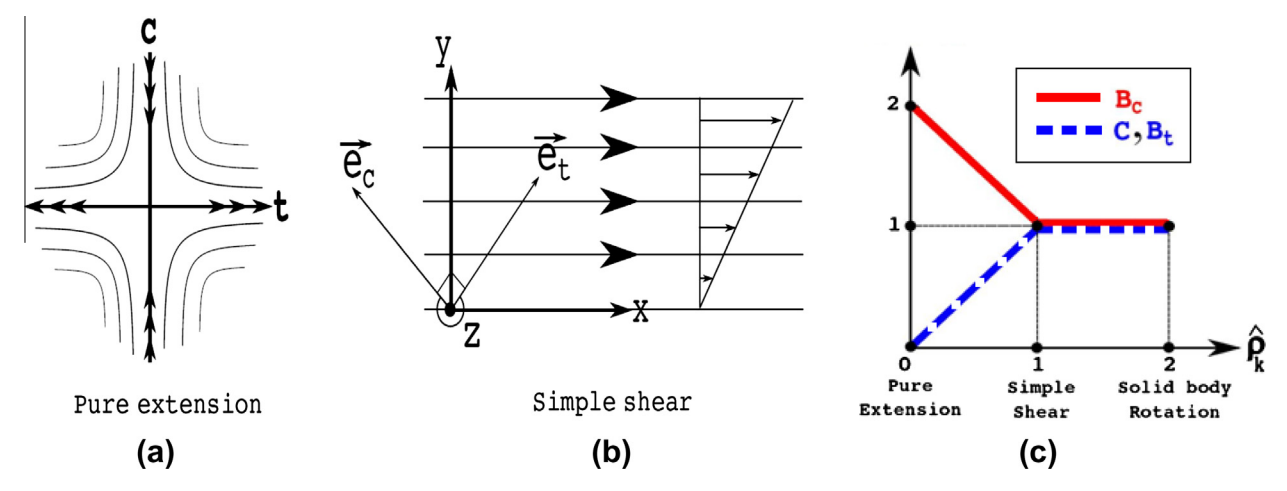


Fig. 11. The compression and tension coordinate system in (a) pure extension and (b) simple shear flows; (c) variation of C, B_t , and B_c with the kinematic ratio $\hat{\rho}_k$.

5.2. Validation: viscous resuspension and two-dimensional mixing

Further validation of the frame-invariant model and the addition of the buoyancy effects is presented here by simulating the two-dimensional resuspension and mixing in a horizontal Couette cell experimentally investigated by Rao et al. [37].

In the experiment, Rao et al. [37] used PMMA particles of radius a = 397 μ m and of density ρ_p^i = 1.18 g cm⁻³, suspended in a newtonian liquid (glycerol/water solution) of density ρ_f^i = 1.253 g cm⁻³ and of viscosity μ_0 = 0.588 Pa s. Measurements of the particle concentration profiles during the de-mixing of an initially 20% well-mixed suspension were performed via the NMR imaging technique. The suspension was placed between two concentric horizontal cylinders with the inner cylinder of radius R_{in} = 0.64 cm and the outer cylinder of radius R_{out} = 2.54 cm (a wide-gap Couette cell) where gravity, before rotating the inner cylinder, acted on the suspension causing the particles to float toward the upper surface of the outer cylinder $\left(\rho_p^i < \rho_f^i\right)$. Then, the suspension was sheared horizontally in the Couette cell by rotating the inner cylinder and the concentration profiles were measured.

The boundary conditions at the initial state and the two-dimensional mesh in the *xy*-plane of this case are presented in Fig. 13a

and b, respectively. As shown in Fig. 13a, the initial bulk concentration over the domain of area S is computed as the area weighted average of the initial concentrations in the two parts of the domain of areas $S_1 = 0.34S$ and $S_2 = 0.66S$ and is given by

$$\frac{S_1}{S} \, \phi_{1-\text{bulk}} + \frac{S_2}{S} \, \phi_{2-\text{bulk}} = \phi_{\text{bulk-initial}} = 0.20 \quad (S = S_1 + S_2), \eqno(52)$$

In the simulations, the parameters of the SBM were assigned the following values:

$$\begin{cases} \eta_{N}(\phi) = 1.08 \left(\frac{\phi}{\phi_{m}}\right)^{2} \left(1 - \frac{\phi}{\phi_{m}}\right)^{-2}, \eta_{s} = \left(1 - \frac{\phi}{\phi_{m}}\right)^{-2}, \\ f(\phi) = \left(1 - \frac{\phi}{\phi_{m}}\right) (1 - \phi)^{\alpha - 1} \\ \phi_{m} = 0.63, \alpha = 4, \lambda_{2} = 0.81 \left(\frac{\phi}{\phi_{m}}\right) + 0.66, \\ \lambda_{3} = -0.0088 \left(\frac{\phi}{\phi_{m}}\right) + 0.54, \quad a_{s} = 0 \end{cases}$$
(53)

The calculation time, using the grid system displayed in Fig. 13b, for any single case was of the order of $t_{calc.} \sim 6$ h under a single **CPU** of 1GHz. The time step was fixed at $\delta t_{calc.}$ = 0.005 that assured a courant number Cr < 1.

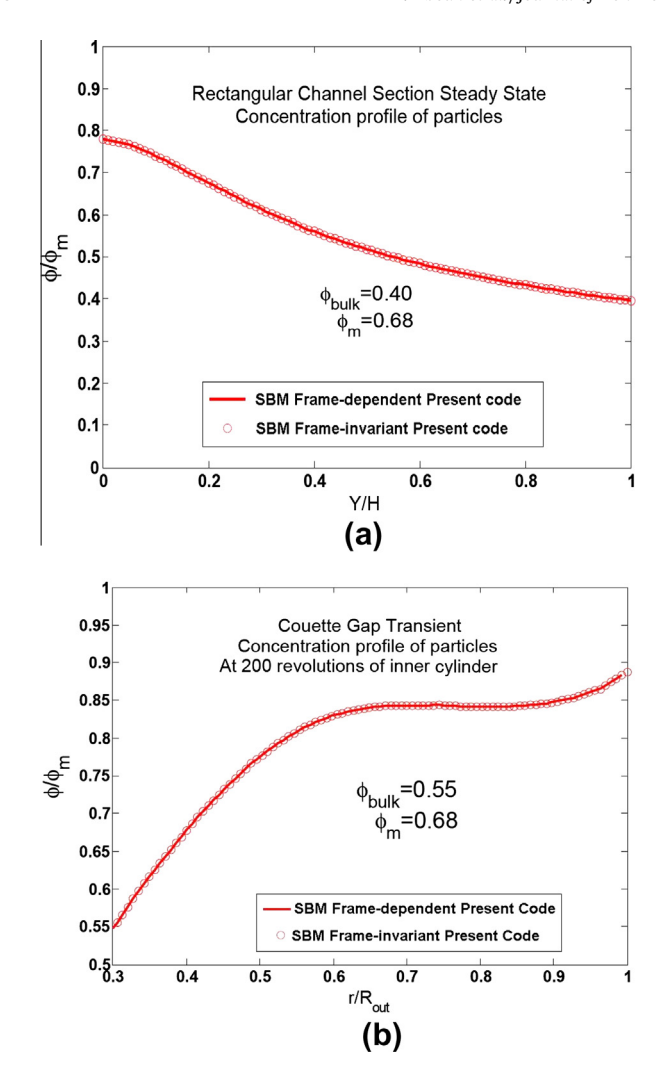


Fig. 12. (a) Comparison of the steady state particle concentration profile obtained using both the frame-dependent and frame-invariant SBM for the suspension flow in a conduit of rectangular cross-section at $\frac{x}{L} = 0.85$ and for $\phi_b = 0.4$; (b) Comparison of the steady state particle concentration profile obtained using both the frame-dependent and frame-invariant SBM for the suspension flow in a Couette cell geometry for $\phi_b = 0.4$.

Maps of the simulated concentration fields are compared in Figs. 14 and 15 with similar ones obtained experimentally by Rao et al. [37] via NMR imaging. Figs. 14a1-d1 and 15a1-d1 show the NMR images of the ϕ fields, while Figs. 14a2-d2 and 15a2d2 display the corresponding simulated fields obtained with the modified SBM. Fig. 14 compares results at turn number 0, 45, 135, and 225 of the inner cylinder, while Fig. 15 presents similar comparisons at turns 315, 405, 495, and 585. As shown good agreements between the experimental and numerical results is obtained. This can be seen more clearly if one, for example, compares the thickness and position of the concentrated zone being mixed with the suspending liquid (red tail in Numerical SBM figures which is near the outer cylinder of the horizontal Couette Cell). Furthermore, an asymmetry in the concentration profiles is observed, which is in accord with experimental measurements and is due to buoyancy effects.

In Eq. (53) a value of 0.63 is used for the maximum packing volume fraction ϕ_m . To justify the use of this value, additional computations were performed to study the effects of the maximum packing volume fraction ϕ_m on mixing in the suspension. For that purpose, the values for the parameters in the SBM were fixed to those in Eq. (53) except for ϕ_m and computations were performed

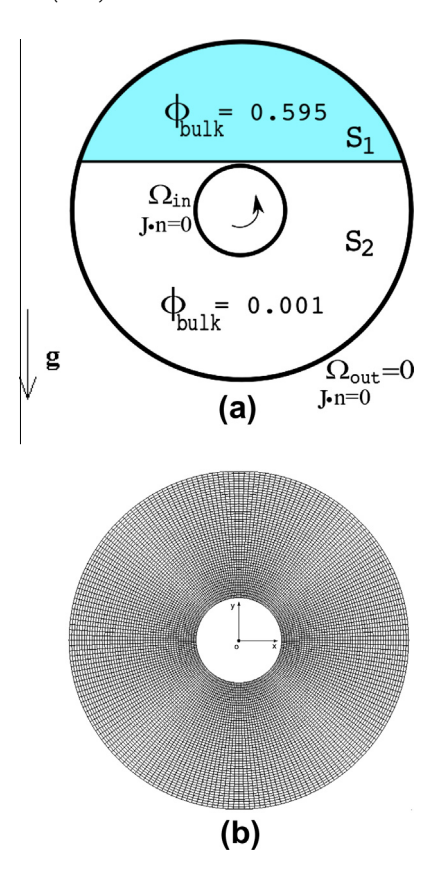


Fig. 13. (a) Schematic of the physical domain and initial and boundary conditions for the viscous re-suspension and two-dimensional mixing problem; (b) the two-dimensional grid system used in the numerical solution of the viscous resuspension and two-dimensional mixing problem.

for two different values of 0.61 and 0.64 assigned for that parameter. The results generated are displayed in Fig. 16a1 and a2 for ϕ_m = 0.61 and in Fig. 16b1 and b2 for ϕ_m = 0.64, respectively. Results after 45 turns of the inner cylinder are shown in Fig. 16a1 and b1 and after 135 turns in Fig. 16a2 and b2. It can be inferred from these figures that numerically mixing occurs either faster or solwer than in the actual experiments depending on the choice of the maximum packing volume fraction value ϕ_m . A higher value of ϕ_m results in mixing occuring earlier than reported experimentally. This is an indication of the importance of ϕ_m in the numerical simulations.

Results reported in Figs. 13 and 14, obtained with a value for ϕ_m = 0.63, are the closest to the experimental NMR data. This is easily seen by comparing both numerical and experimental profiles at the early stages of mixing (i.e. after 45 turns of the inner cylinder shown in Fig. 14a2 and b2). The choice made for this last value of ϕ_m stays always reasonable since it lies between 0.58 and 0.64 which are the only two values for ϕ_m reported by Rao et al. [37] without any measurement. Moreover, the reported maximum packing volume fraction ϕ_m for suspensions of hard spheres has been varying in the literature between 0.58 and 0.72. This range of ϕ_m was either by choice or based on some old measurements of the settling-velocity in resuspension and batch sedimentation experiments, or just by measuring the suspension viscosity, which is fitted by a mathematical law that diverges at a certain value of ϕ_m . The value of ϕ_m depends sharply on the surface roughness of the hard spheres being studied. This surface roughness affects well the interaction between the particles and thus the microstructure orientation which induces a further effect on the global behavior of the suspension (migration) during the flow [2].

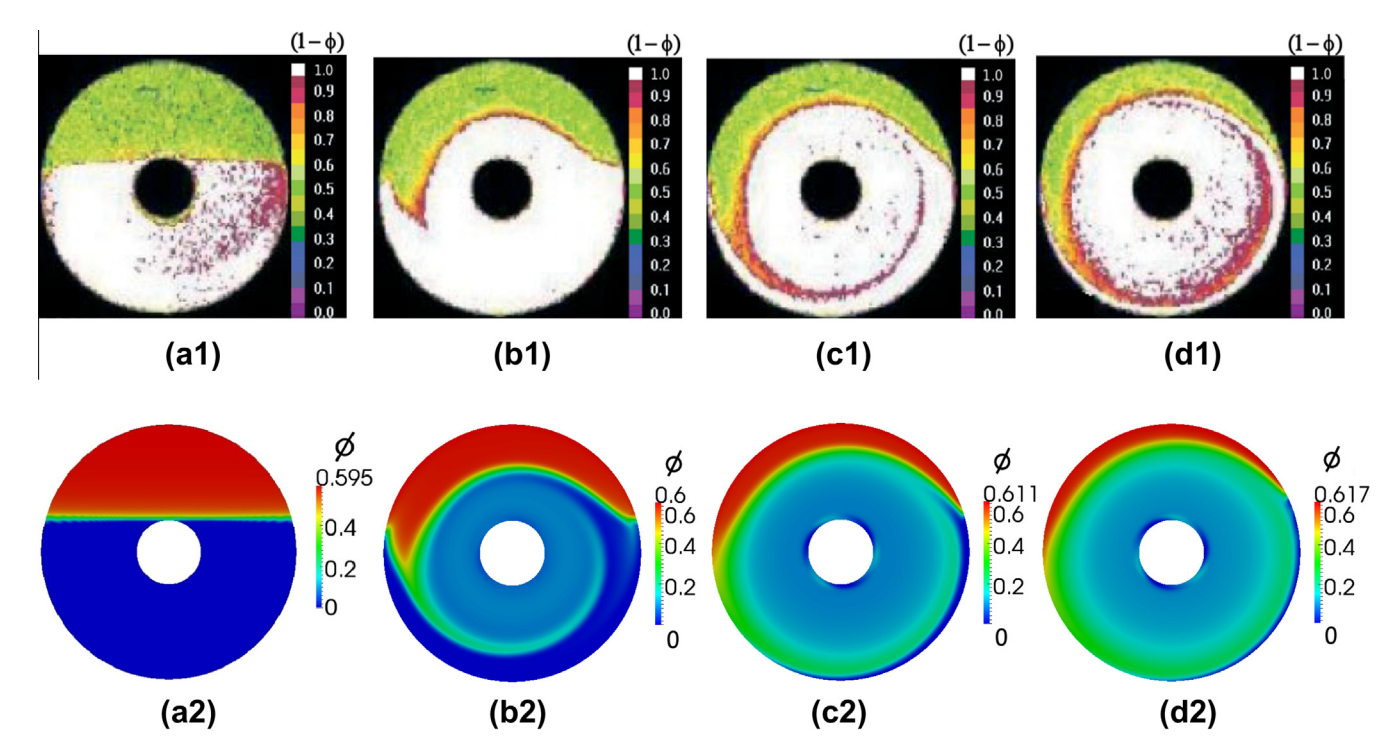


Fig. 14. Comparison of the particle concentration maps obtained experimentally using NMR imaging (a1)–(d1) with numerical ones (a2)–(d2) obtained using the modified SBM with buoyancy effects at [(a1),(a2)] 0, [(b1),(b2)] 45, [(c1),(c2)] 135, and [(d1),(d2)] 225 turns of the inner cylinder for the viscous re-suspension and two-dimensional mixing problem.

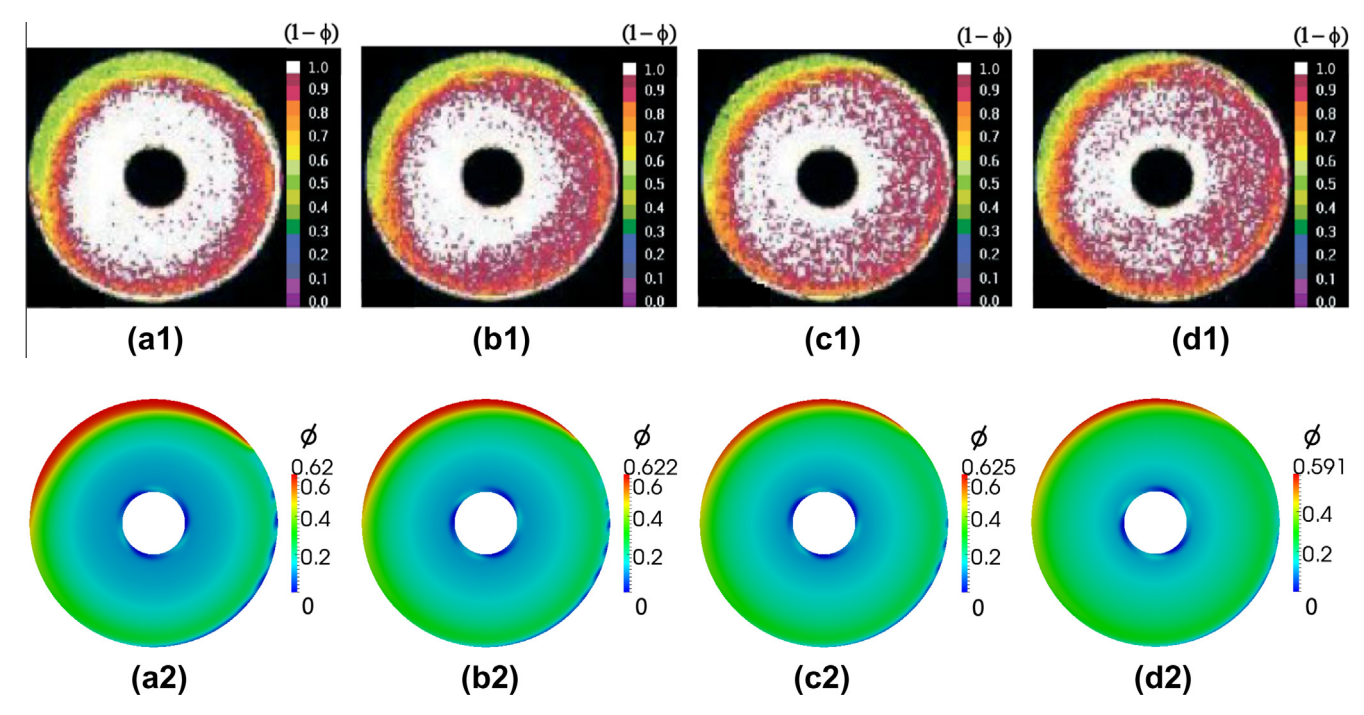


Fig. 15. Comparison of the particle concentration maps obtained experimentally using NMR imaging (a1)–(d1) with numerical ones (a2)–(d2) obtained using the modified SBM with buoyancy effects at [(a1),(a2)] 315, [(b1),(b2)] 405, [(c1),(c2)] 495, and [(d1),(d2)] 585 turns of the inner cylinder for the viscous re-suspension and two-dimensional mixing problem.

The capturing by the SBM of the different physical features involved in this problem (Figs. 14 and 15) is good despite the fact that a two-dimensional model is used to solve a real three-dimensional problem (the Couette Cell here is considered of infinite length in the horizontal direction). Nevertheless,

it will be interesting to simulate more problems in the near future using this two-dimensional frame-invariant SBM (including buoyancy effects) in order to further study suspension flows of non-Brownian hard spheres in more complex geometries.

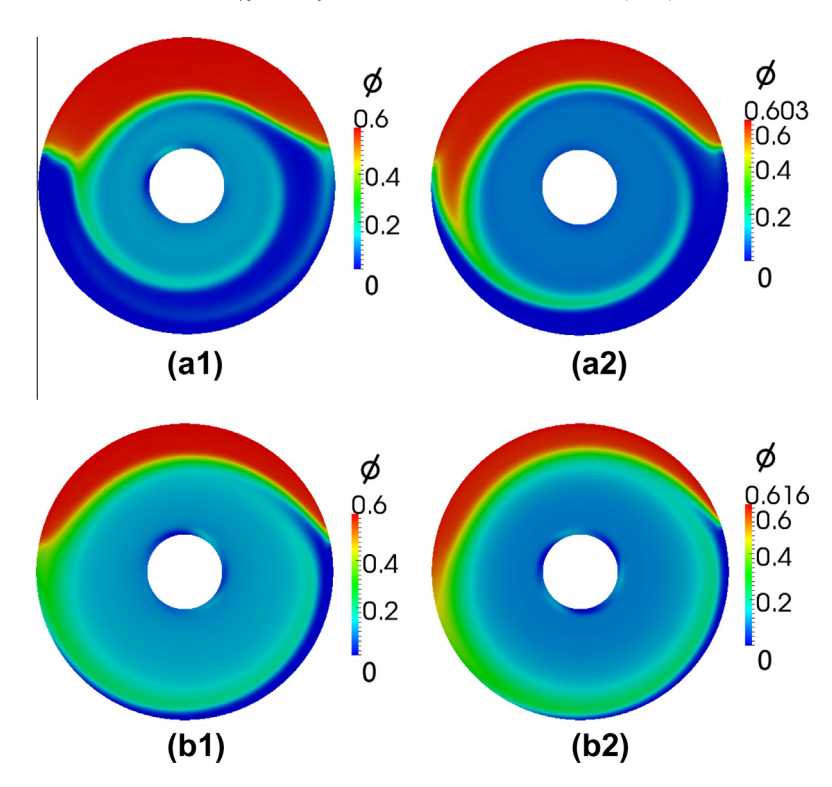


Fig. 16. Numerical concentration maps obtained using the modified SBM with buoyancy effects, for the viscous re-suspension and two-dimensional mixing problem, after [(a1),(b1)] 45 and [(a2),(b2)] 135 turns of the inner cylinder for $\phi_m = 0.61$ [(a1),(a2)] and $\phi_m = 0.64$ [(b1),(b2)].

6. Closing remarks

The coefficients of the two-dimensional Suspension Balance Model (SBM) of Nott and Brady [32] and Morris and Boulay [29] were modified based on recently performed measurements [11]. In these measurements it was found that the normal stress differences in these suspensions are such that $N_2 < 0$ and $N_1 > 0$. This finding of a positive N_1 is in contradiction with all reported results in the literature. However, this was found to have little effect on the model predictions for the shear-induced particle migration in simple shear flows. In addition, measured values resulted in a higher value of K_N = 1.08 compared to the value K_N = 0.75 that was used previously by Morris and Boulay [29]. Moreover, it was also found that λ_2 and λ_3 are not constants as it was assumed previously, but are dependent on the volume fraction of particles ϕ . The twodimensional SBM was implemented in "OpenFOAM®" [34] and was shown to capture well the physical features involved in the shear-induced particle migration in simple shear flows. In fact, numerical results obtained with the modified coefficients suggest that the simplification introduced by Morris and Boulay [29] of assigning constant values to λ_2 and λ_3 in the SBM, rather than considering them functions of ϕ , is appropriate. Furthermore, the value of the measured normal stress viscosity coefficient K_N is not far away from the one previously used in the SBM.

The two-dimensional model was extended into a frame-invariant environment and implemented also in "OpenFOAM®". The frame-invariant model, capable of dealing with general geometries, was extended to include buoyancy effects. Results predicted by the model indicated that it can capture well the physical features involved in the shear-induced particle migration even in geometries where the flow of the suspension is general, and where buoyancy is present. This was demonstrated by solving numerically the two-dimensional resuspension and mixing in a horizontal Couette Cell problem and comparing simulation results with measured data. Finally, it can be stated safely that the two-dimensional model

described well the physical behavior of the different suspension flows simulated in this paper, and could be tested further by simulating additional general flows in more complex geometries.

Acknowledgments

This work was supported by the ANR program (French: ANR-08-BLAN-0048-CSD 2), and the CEDRE program (French-Lebanese: Cooperation for the Evaluation and Development of Research).

References

- [1] R.B. Bird, R.C. Armstrong, O. Hassager, Dynamics of Polymeric Liquids, vol. 1 Fluid Mechanics, vol. 2, Kinetic Theory, Copyright © John Wiley & Sons, Inc., 1987.
- [2] F. Blanc, F. Peters, E. Lemaire, Experimental Signature of the Pair-Trajectories of Rough Spheres in the Pair Distribution Function of Dilute Sheared Non-Colloidal Suspensions, PRL, Physical Review Letters, October 2011.
- [3] F. Boyer, O. Pouliquen, E. Guazzelli, Dense suspensions in rotating-rod flows: normal stresses and particle migration, J. Fluid Mech. 272 (2011).
- [4] F. Boyer, O. Pouliquen, E. Guazzelli, Unifying suspension and granular rheology, PRL, 2011.
- [5] J.F. Brady, J.F. Morris, Microstructure of strongly sheared suspensions and its impact on rheology and diffusion, J. Fluid Mech. 348 (1997) 103–139.
- [6] J. Crank, P. Nicolson, A practical method for numerical evaluation of solutions of partial differential equations of the heat-conduction type, Proceedings of the Cambridge Philosophical Society 43 (1947) 50–67.
- [7] B. Chapman, Sshear-Induced Migration Phenomena in Concentrated Suspensions, Ph.D. Thesis, University of Notre Dame, 1990.
- [8] E. Couturier, F. Boyer, O. Pouliquen, E. Guazelli, Suspensions in a tilted trough: second normal stress difference, J. Fluid Mech. 686 (2011) 26–39.
- [9] R.H. Davis, A. Acrivos, Sedimentation of non- colloidal particles at low Reynolds numbers, Annu. Rev. Fluid Mech. 17 (1985) 91–118.
- [10] T. Dbouk, Rheology Of Concentrated Suspensions & Shear-Induced Migration, Ph.D. Thesis, University Of Nice Sophia Antipolis, 2012.
- [11] T. Dbouk, L. Lobry, E. Lemaire, Normal stresses in concentrated non-Brownian suspensions, J. Fluid Mech. 715 (2013) 239–272.
- [12] A. Deboeuf, Interactions hydrodynamiques dans les suspensions macroscopiques, Ph.D. thesis, Pierre and Marie Curie University, 2008.
- [13] A. Deboeuf, G. Gauthier, J. Martin, Y. Yurkovetsky, J. Morris, Particle pressure in a sheared suspension: a bridge from osmosis to granular dilatancy, Phys. Rev. Lett. 102 (2009) 108301.

- [14] D.A. Drew, R.T. Lahey, Analytical modeling of multiphase flow, in: M. Roco (Ed.), Particulate Two-Phase Flows, Butterworth-Heinemann, Boston, 1993.
- [15] Z. Fang, A. Mammoli, J.F. Brady, M.S. Ingber, L.A. Mondy, A.L. Graham, Flow-aligned tensor models for suspension flows, Int. J. Multiphase Flow 28 (1) (2002) 137–166.
- [16] F.A. Gadala-Maria, The Rheology of Concentrated Suspension, Ph.D. thesis, Stanford University, 1979.
- [17] F. Gadala-Maria, A. Acrivos, A. Shear-induced structure in a concentrated suspension of solid spheres, J. Rheol. 24 (1980) 799.
- [18] H.L. Goldsmith, S.G. Mason, The microrheology of dispersions, in: F.R. Eirich (Ed.), Rheology Theory and Applications, vol. 4, Academic, 1967, pp. 86–246.
- [19] D. Leighton, A. Acrivos, Viscous resuspension, Chem. Eng. Sci. 41 (1986) 1377– 1384
- [20] D. Leighton, A. Acrivos, Measurement of self- diffusion in concentrated suspensions of spheres, J. Fluid Mech. 177 (1987) 109–131.
- [21] D. Leighton, A. Acrivos, The shear-induced migration of particles in concentrated suspensions, J. Fluid Mech. 181 (1987) 415–439.
- [22] D. Lhuillier, Migration of rigid particles in non-Brownian viscous suspensions, Phys. Fluids 21 (2009) 023302.
- [23] M.K. Lyon, L.G. Leal, An experimental study of the motion of concentrated suspensions in two-dimensional channel flow, Part 1. Monodisperse systems, J. Fluid Mech. 363 (1998) 25–56.
- [24] S.H. Maron, P.E. Pierce, Application of free-eyring generalized flow theory to suspensions of spherical particles, J. Colloid. Sci. 11 (1956) 162–170.
- [25] D. Merhi, E. Lemaire, G. Bossis, F. Moukalled, Particle migration in a concentrated suspension flowing between rotating parallel plates: investigation of diffusion flux coeffcients, J. Rheol. 49 (2005) 1429–1448.
- [26] R.M. Miller, Continuum Modeling of Liquid-Solid Suspensions for Nonviscometric Flows, Ph.D. thesis, School of Chemical & Biomolecular Engineering, Georgia Institute of Technology, 2004.
- [27] R.M. Miller, J.F. Morris, Normal stress-driven migration and axial development in pressure-driven flow of concentrated suspensions, J. Non-Newton. Fluid Mech. 135 (2006) 149–165.
- [28] R.M. Miller, J.P. Singh, J.F. Morris, Suspension flow modeling for general geometries, Chem. Eng. Sci. 64 (2009) 4597–4610.
- [29] J.F. Morris, F. Boulay, Curvilinear flows of non-colloidal suspensions: the role of normal stresses, J. Rheol. 43 (5) (1999) 1213–1237.
- [30] J.F. Morris, J.F. Brady, Pressure-driven flow of a suspension: Buoyancy effects, Int. J. Multiphase Flow 24 (1) (1998) 105–130.

- [31] J.F. Morris, B. Katyal, Microstructure from simulated Brownian suspension flows at large shear rate, Phys. Fluids 14 (2002) 1920.
- [32] P.R. Nott, J.F. Brady, Pressure-driven flow of suspensions: simulation and theory, J. Fluid Mech. 275 (1994) 157–199.
- [33] P.R. Nott, E. Guazzelli, O. Pouliquen, The suspension balance model revisited, Phys. Fluids 23 (2011) 043304.
- [34] OpenFOAM® project web pages http://www.openfoam.com>.
- [35] S.V. Patankar, Numerical Heat Transfer and Fluid Flow, Hemisphere, New York, 1980.
- [36] R.J. Phillips, R.C. Armstrong, R.A. Brown, A. Graham, J.R. Abbott, A constitutive model for concentrated suspensions that accounts for shear-induced particle migration, Phys. Fluids A 4 (1992) 30–40.
- [37] R. Rao, L. Mondy, A. Sun, S. Altobelli, A numerical and experimental study of batch sedimentation and viscous resuspension, Int. J. Numer. Meth. Fluids 39 (2002) 465–483.
- [38] C.M. Rhie, W.L. Chow, A numerical study of theturbulent flow past and airfoil with trailing edge separation, AIAA J. 21 (1983) 1525–1532.
- [39] J.F. Richardson, W.N. Zaki, Sedimentation and fluidization: Part I, Trans. Inst. Chem. Eng. 32 (1954) 35–47.
- [40] E. Ryssel, P.O. Brunn, Comparison of a quasi-Newtonian fluid with a viscoelastic fluid in planar contraction flow, J. Non-Newton. Fluid Mech. 86 (1999) 309–335.
- [41] U. Schaflinger, A. Acrivos, K. Zhang, Viscous resuspension of a sediment within a laminar and stratified flow, Int. J. Multiphase Flow 16 (1990) 567–578.
- [42] P.R. Schunk, L.E. Scriven, Constitutive equation for modeling mixed extension and shear in polymer solution processing, J. Rheol. 34 (7) (1990).
- [43] A. Sierou, J.F. Brady, Rheology and microstructure in concentrated noncolloidal suspensions, J. Rheol. 46 (2002) 1031.
- [44] A. Singh, P.R. Nott, Experimental measurements of the normal stresses in sheared Stokesian suspensions, J. Fluid Mech. 490 (2003) 293–320.
- [45] K. Yeo, M.R. Maxey, Simulation of concentrated suspensions using the force-coupling method, J. Comput. Phys. 229 (2010) 2401–2421.
- [46] K. Yeo, M.R. Maxey, Dynamics of concentrated suspensions of non-colloidal particles in Couette flow, J. Fluid Mech. 649 (2010) 205231.
- [47] Y. Yurkovetsky, J.F. Morris, Particle pressure in a sheared Brownian suspension, J. Rheol. 52 (2008) 141.
- [48] I.E. Zarraga, D.A. Hill, D.T. Leighton, The characterization of the total stress of concentrated suspensions of noncolloidal spheres in Newtonian fluids, J. Rheol. 44 (2000) 185–220.